Open access • Journal Article • DOI:10.1142/S0218202508003066

Allen-Cahn systems with volume constraints — Source link

Harald Garcke, Britta Nestler, Björn Stinner, Frank Wendler

Institutions: University of Regensburg, University of Sussex

Published on: 01 Aug 2008 - Mathematical Models and Methods in Applied Sciences (World Scientific Publishing Company)

Topics: Finite difference and Curvature

Universität Regensburg
Mathematik

Allen-Cahn systems with volume constraints

Harald Garcke, Britta Nestler, Björn Stinner
and Frank Wendler

Preprint Nr. 14/2007

Mathematical Models and Methods in Applied Sciences

Allen-Cahn systems with volume constraints

HARALD GARCKE
NWF I - Mathematik, Universität Regensburg
D–93040 Regensburg, Germany
harald.garcke@mathematik.uni-regensburg.de

BRITTA NESTLER
Fachbereich Informatik, HS Karlsruhe
Moltkestr. 30, 76133 Karlsruhe
britta.nestler@hs-karlsruhe.de

BJÖRN STINNER
Department of Mathematics, University of Sussex
Mantell Building, Falmer, BN1 9RF, United Kingdom
bs68@sussex.ac.uk

FRANK WENDLER
Fachbereich Informatik, HS Karlsruhe
Moltkestr. 30, 76133 Karlsruhe
frank.wendler@hs-karlsruhe.de

Received (Day Month Year)
Revised (Day Month Year)
Communicated by (xxxxxxxxxx)

We consider the evolution of a multi-phase system where the motion of the interfaces is driven by anisotropic curvature and some of the phases are subject to volume constraints. The dynamics of the phase boundaries is modeled by a system of Allen-Cahn type equations for phase field variables resulting from a gradient flow of an appropriate Ginzburg-Landau type energy. Several ideas are presented in order to guarantee the additional volume constraints. Numerical algorithms based on explicit finite difference methods are developed, and simulations are performed in order to study local minima of the system energy. Wulff shapes can be recovered, i.e., energy minimizing forms for anisotropic surface energies enclosing a given volume. Further applications range from foam structures or bubble clusters to tessellation problems in two and three space dimensions.

Keywords: phase field; finite differences; semi-smooth Newton method.

AMS Subject Classification: 49Q20, 74P20, 65M06,

1. Introduction

Evolution laws decreasing the interfacial energy of a multi-phase system appear frequently in physics and materials science. In this article, we study cases in which some of the phases fulfill volume constraints. Such a situation occurs, e.g., in shape evolution of crystals with surface attachment limited kinetics[4] where the material is rearranged in order to decrease the crystalline surface energy. Another example is the determination of foam structures by prescribing the area or volume (in two or three space dimensions respectively) of the foam bubbles and minimizing the length or area of the separating lines or hypersurfaces. A related problem is the famous honeycomb conjecture[19]. Let us more precisely state the situations we want to investigate.

Consider a domain in the two or three dimensional space that is subdivided into $M \in \mathbb{N}$ sub-domains. The sub-domains, denoted by Ω_α, $\alpha = 1, \ldots, M$, need not to be connected and will be interpreted as different phases throughout this paper. The interfaces separating the phases are assumed to be smooth hypersurfaces. Given two indices $\alpha \neq \beta$ the interfaces between the corresponding phases are denoted by $\Gamma_{\alpha\beta}$. We postulate a system energy of the form

$$\mathcal{F}_{SI} = \sum_{\alpha<\beta} \int_{\Gamma_{\alpha\beta}} \gamma_{\alpha\beta}(\boldsymbol{\nu}_{\alpha\beta}) d\mathcal{H}^{d-1}. \tag{1.1}$$

Here, the vector $\boldsymbol{\nu}_{\alpha\beta}$ denotes the unit normal on $\Gamma_{\alpha\beta}$ pointing into Ω_β. The surface energy densities $\gamma_{\alpha\beta}$ are positive functions of the unit normal and, therefore, allow to take anisotropy on the phase interfaces into account. Finally, $d\mathcal{H}^{d-1}$ stands for the integration with respect to a $(d-1)$-dimensional surface measure.

Minimizers of the system energy (1.1) and the evolution according to an L^2 gradient flow of the above energy are of interest where, in addition, the phases $1, \ldots, A$ for some number $A \in \{1, \ldots, M\}$ are due to additional volume constraints

$$|\Omega_\alpha| := \text{volume}(\Omega_\alpha) = M_\alpha, \quad \alpha = 1, \ldots, A, \tag{1.2}$$

with appropriate numbers $M_\alpha \in (0, |\Omega|)$. As we will see in the following section, the gradient flow leads to a weighted mean curvature flow in the sense of Ref. 17 with additional forcing terms ensuring the volume conditions for the phases. This motion is coupled to angle conditions for the interfaces in triple points or lines, i.e., in points where three phase interfaces meet.

In this article we present a model for such a system which is based on the phase field approach. To every phase we assign a phase field variable $\phi_\alpha(\boldsymbol{x})$, $\alpha = 1, \ldots, M$, representing the presence of the corresponding phase in some point $\boldsymbol{x} \in \Omega$. This means that the variables fulfill $\phi_\alpha(\boldsymbol{x}) \in [0, 1]$ and sum up to give 1, i.e., the vector of the phase fields is demanded to lie on the Gibbs simplex Σ^M,

$$\boldsymbol{\phi}(\boldsymbol{x}) \in \Sigma^M := \Big\{ \boldsymbol{\zeta} = (\zeta_1, \ldots, \zeta_M) \in \mathbb{R}^M \Big| \sum_{\alpha=1}^{M} \zeta_\alpha = 1, \;\; \zeta_\alpha \geq 0, \, \alpha = 1, \ldots, M \Big\}. \tag{1.3}$$

Observe that the corners of Σ^M precisely are the points where one of the components equals 1 and the others vanish, i.e., the corners correspond to the pure phases.

The system energy of the diffuse interface approach is defined to be the following Ginzburg-Landau functional:

$$\mathcal{F}_{GL}(\boldsymbol{\phi}) = \int_\Omega \big(\varepsilon a(\boldsymbol{\phi}, \nabla\boldsymbol{\phi}) + \frac{1}{\varepsilon} w(\boldsymbol{\phi})\big) dx. \tag{1.4}$$

The function w is a multi-well potential with global minima in the corners of Σ^M. Hence, for a state function $\boldsymbol{\phi}$ it is energetically advantageous to take values close to the minima of w. This leads to a separation of the domain into different phases. But there may be transition regions where $\boldsymbol{\phi}$ changes from one minimum to another. The potential a penalizes gradients, the simplest choice being $a(\boldsymbol{\phi}, \nabla\boldsymbol{\phi}) = |\nabla\boldsymbol{\phi}|^2$. Therefore, it prevents $\boldsymbol{\phi}$ from changing in a too thin transition region. Indeed, it turns out that the thickness of the transition region is of order ε which is a small length scale appearing in (1.4). The volume conditions (1.3) now read

$$\int_\Omega \phi_\alpha = M_\alpha, \quad \alpha = 1, \dots, A. \tag{1.5}$$

Again we are interested in (local) minimizers of the above energy and consider the gradient flow of (1.4) with respect to a possibly weighted L^2 inner product. The dynamic problem leads to a system of Allen-Cahn equations for the phase field variables which corresponds to a diffuse interface version of weighted mean curvature flow. Non-local terms that can be seen as additional forcing terms enter the parabolic differential equations and change the speed of the phase interfaces in such a way that (1.5) is satisfied during the relaxation.

For the case of two phases, i.e., $M = 2$, the phase field approach to the considered problem has been discussed in Ref. 16. Using matched asymptotic expansions and multiple timescales, it is shown that the description with moving hypersurfaces, i.e., the sharp interface model, comes out in the limit when the diffuse interface thickness, which scales with ε, converges to zero. In certain situations this limiting behavior could even be rigorously established[3]. But effects on the ε-scale that vanish in the limit can indeed influence the long time behavior of solutions to the diffuse interface model[21].

In contrast to the above references we face arbitrary numbers of phases. We present several methods to incorporate the non-local terms. The developed algorithms are based on finite difference methods to approximate solutions to the non-local parabolic equations. For calibration reasons with respect to surface energies[7] we are strongly interested in multi-well potentials w of obstacle type, i.e., w is real valued only on Σ^M but set to ∞ if the argument $\boldsymbol{\phi}$ does not belong Σ^M. One task is then to ensure that the forcing terms are present only within the interfacial regions. Moreover, it is a nontrivial task to find the correct strength of the additional forces.

In an ad hoc method we let the phase interfaces move according to the gradient flow of (1.4) and then, in a second step, compute the change of volume and add values equilibrating it. The use of the obstacle potential necessitates to iterate the

equilibration procedure of the second step. Another idea is to apply the Newton method to compute the necessary forces. Because of the obstacle potential the function of which the roots are to be found is not differentiable, but it turns out that it provides enough regularity so that a semi-smooth method in the sense of Ref. 15 converges. For the analytical results certain regularity assumption on the gradient energy a are necessary. They are not fulfilled in the case of crystalline surface energies leading to crystalline curvature flow[17]. But numerical tests revealed that the developed methods are still applicable.

The models will precisely be stated in the the following section. In particular, the decay of energy is analyzed. In the third section the procedures are stated and investigated. The main result concerns the convergence of the Newton method. Finally, the last section deals with numerical simulations using the developed algorithms. Tests and applications concern the evolution of two spheres, clusters of bubbles and the construction of tessellations on a prescribed periodicity cell.

2. Modeling

Throughout this section, let $\Omega \subset \mathbb{R}^d$ with $d \in \{2,3\}$ be a connected open set with piecewise smooth boundary and external unit normal $\boldsymbol{\nu}_{ext}$ on $\partial\Omega$, and let $I = (0,\mathcal{T})$ with $\mathcal{T} \in (0,\infty]$ be a time interval.

2.1. *Sharp interface model*

2.1.1. *Notation and governing equations*

The domain Ω is subdivided into M time dependent sub-domains $\Omega_\alpha(t)$, $\alpha = 1,\dots,M$, separated by moving interfaces $\Gamma_{\alpha\beta}(t)$ with unit normal $\boldsymbol{\nu}_{\alpha\beta}$ pointing into Ω_β. Here and in the following the time dependence of the phases and the phase interfaces will not be stated explicitly any more. The phase interfaces end in points belonging to the sets $T_{\alpha\beta\delta} := \overline{\Gamma}_{\alpha\beta} \cap \overline{\Gamma}_{\beta\delta} \cap \overline{\Gamma}_{\delta\alpha}$ or $\Gamma_{\alpha\beta,ext} := \overline{\Gamma}_{\alpha\beta} \cap \partial\Omega$. The following equations and identities are restricted to times $t \in I$ when we are in the following situation: the phase interfaces $\Gamma_{\alpha\beta}$ are smooth and, hence, measurable with respect to the surface measure $\mathcal{H}^{d-1}$, and to arbitrary indices α, β there is a chain of indices $\alpha = \eta_1, \eta_2, \dots, \eta_n = \beta$ such that each set $\Gamma_{\eta_i\eta_{i+1}}$ has positive $\mathcal{H}^{d-1}$-measure. The fact that the domain Ω is connected certainly enables to weaken the last assumption but we do not want to discuss this issue here in detail.

To describe the energy of the system we introduce surface energy densities $\gamma_{\alpha\beta} : S^{d-1} \to (0,\infty)$ where $S^{d-1} \subset \mathbb{R}^d$ is the $(d-1)$-dimensional unit sphere. By one-homogeneous extension, i.e., setting $\gamma_{\alpha\beta}(r\boldsymbol{\nu}) := r\gamma_{\alpha\beta}(\boldsymbol{\nu})$ for all $r \geq 0$, $\boldsymbol{\nu} \in S^{d-1}$, the surface energy densities become functions on $\mathbb{R}^d$. They are assumed to be convex and smooth (except in zero), and for consistency reasons we assume that $\gamma_{\beta\alpha}(\boldsymbol{\nu}) = \gamma_{\alpha\beta}(-\boldsymbol{\nu})$. To avoid wetting effects we suppose that

$$\gamma_{\alpha\beta}(\boldsymbol{\nu}) + \gamma_{\beta\delta}(\boldsymbol{\nu}) > \gamma_{\alpha\delta}(\boldsymbol{\nu}) \text{ for mutually different } \alpha,\beta,\delta \text{ and all } \boldsymbol{\nu} \in S^{d-1}.$$

To have volume constraints for the phases with indices $\alpha = 1, \dots, A$ means that the constraints (1.2) are fulfilled. The numbers M_α are positive and fulfill $\sum_{\alpha=1}^{A} M_\alpha < |\Omega|$ in the case $A < M$ and $\sum_{\alpha=1}^{A} M_\alpha = |\Omega|$ in the case $A = M$ respectively.

The evolution of the system is defined by a gradient flow of the energy (1.1) with respect to a weighted L^2 inner product, taking the constraints (1.2) with the help of Lagrange factors μ_α, $\alpha = 1, \dots, A$, into account. In the following, we state the resulting equations. The derivation is sketched in the appendix.

The phase interfaces $\Gamma_{\alpha\beta}$ move according to the laws

$$m_{\alpha\beta} v_{\alpha\beta} = -\nabla_s \cdot \big(D\gamma_{\alpha\beta}(\boldsymbol{\nu}_{\alpha\beta})\big) + (\mu_\beta - \mu_\alpha). \tag{2.1}$$

Here, $v_{\alpha\beta}$ is the normal velocity in direction $\boldsymbol{\nu}_{\alpha\beta}$, and the $m_{\alpha\beta} = m_{\beta\alpha}$ are positive kinetic coefficients. A kinetic anisotropy can easily be taken into account, i.e., each $m_{\alpha\beta}$ is a function of $\boldsymbol{\nu}_{\alpha\beta}$ so that the velocity of the phase interface $\Gamma_{\alpha\beta}$ is enhanced or restricted in certain spacial directions. The operator $\nabla_s \cdot$ stands for the surface divergence, and $D\gamma_{\alpha\beta}$ denotes the derivative of $\gamma_{\alpha\beta}$. We have set

$$\mu_\alpha := 0 \quad \text{if } \alpha > A \tag{2.2}$$

for shorter presentation. The Lagrange factors can be considered as bulk forces acting on the phase interfaces and influencing its motion, whence they will be referred as forcing terms in the following. They can be computed from the constraints (1.2) which is shown in the next subsection. The terms $-\nabla_s \cdot D\gamma_{\alpha\beta}$ are commonly called weighted mean curvature[17], whence (2.1) can be understood as weighted mean curvature flow for the phase interfaces with additional forcing terms due to the volume constraints.

The equations of motion (2.1) are supplied with boundary conditions in points where the phase interfaces meet the external boundary of Ω or end in triple points belonging to the sets $T_{\alpha\beta\delta}$. As shown in the appendix, they follow from the definition of the evolution as gradient flow of (1.1), but they can also be considered as due to mechanical equilibrium and are commonly known as Youngs's law (cf. Ref. 12 and Ref. 9 and the references therein). The external unit normal to Γ_{ik} in a point $\boldsymbol{x} \in T_{\alpha\beta\delta}$ is denoted by $\boldsymbol{\tau}_{ik}$, $(i,k) \in \mathcal{A}_{\alpha\beta\delta} := \{(\alpha,\beta),(\beta,\delta),(\delta,\alpha)\}$. The condition in $\boldsymbol{x}$ now reads

$$0 = \sum_{(i,k)\in\mathcal{A}_{\alpha\beta\delta}} -(D\gamma_{ik}(\boldsymbol{\nu}_{ik}) \cdot \boldsymbol{\tau}_{ik})\boldsymbol{\nu}_{ik} + \gamma_{ik}(\boldsymbol{\nu}_{ik})\boldsymbol{\tau}_{ik}. \tag{2.3}$$

In the case $d = 2$ the condition is the same and can be derived by identically extending the local situation into the third dimension. The condition implies that certain angles are formed.

Similarly, there are angle conditions in points where an interface meets the external boundary, i.e., in the sets $\Gamma_{\alpha\beta,ext}$:

$$0 = \gamma_{\alpha\beta}(\boldsymbol{\nu}_{\alpha\beta})(\boldsymbol{\nu}_{\alpha\beta} \cdot \boldsymbol{\nu}_{ext}) + (D\gamma_{\alpha\beta}(\boldsymbol{\nu}_{\alpha\beta}) \cdot \boldsymbol{\tau}_{\alpha\beta})(\boldsymbol{\tau}_{\alpha\beta} \cdot \boldsymbol{\nu}_{ext}) \tag{2.4}$$

where again $\boldsymbol{\tau}_{\alpha\beta}$ denotes the external unit normal to $\Gamma_{\alpha\beta}$ on $\Gamma_{\alpha\beta,ext}$.

The forcing terms in the motion law (2.1) act against volume changes of a phase due to a local interface motion by a force acting globally on the whole boundary of the phase. It is worth to remark that, because of the kinetic coefficients $m_{\alpha\beta}$, the influence of the forcing on the normal velocity depends on the type of the phase interface. If the kinetic coefficients $m_{\alpha\beta}(\boldsymbol{\nu}_{\alpha\beta})$ are anisotropic it even depends on the directions of the interfaces.

2.1.2. *Computation of the forcing terms*

For shorter presentation, let us set

$$\Gamma_{\alpha\alpha} := \emptyset, \quad m_{\alpha\alpha} := 1, \qquad \alpha = 1, \dots, M.$$

Condition (1.2) yields for all $\beta = 1, \dots, A$ that

$$\begin{aligned} 0 = \partial_t |\Omega_\beta| &= \sum_{\alpha=1}^{M} \int_{\Gamma_{\alpha\beta}} (-v_{\alpha\beta}) d\mathcal{H}^{d-1} \qquad (2.5) \\ &= \sum_{\alpha=1}^{M} \left(\int_{\Gamma_{\alpha\beta}} \frac{\nabla_s \cdot (D\gamma_{\alpha\beta}(\boldsymbol{\nu}_{\alpha\beta}))}{m_{\alpha\beta}} d\mathcal{H}^{d-1} + (\mu_\alpha - \mu_\beta) \int_{\Gamma_{\alpha\beta}} \frac{1}{m_{\alpha\beta}} d\mathcal{H}^{d-1} \right) \end{aligned}$$

For $\alpha, \beta = 1, \dots, M$ let us introduce the abbreviations

$$\begin{aligned} \kappa_\beta &:= \sum_{\alpha=1}^{M} \int_{\Gamma_{\alpha\beta}} \frac{\nabla_s \cdot (D\gamma_{\alpha\beta}(\boldsymbol{\nu}_{\alpha\beta}))}{m_{\alpha\beta}} d\mathcal{H}^{d-1}, \\ g_{\alpha\beta} &:= \int_{\Gamma_{\alpha\beta}} \frac{1}{m_{\alpha\beta}} d\mathcal{H}^{d-1} \quad = \quad g_{\beta\alpha} \geq 0, \\ h_{\beta\beta} &:= \sum_{\delta=1}^{M} g_{\beta\delta}, \\ h_{\beta\alpha} &:= -g_{\beta\alpha} \quad \text{if } \alpha \neq \beta \end{aligned}$$

and let us set

$$\boldsymbol{H} := (h_{\beta\alpha})_{\beta,\alpha=1}^{A,M}, \quad \boldsymbol{\kappa} := (\kappa_\beta)_{\beta=1}^{A}.$$

Then (2.5) corresponds to the linear system $\boldsymbol{H}\boldsymbol{\mu} = \boldsymbol{\kappa}$ (remember that $\mu_\alpha = 0$ if $\alpha > A$), i.e.,

$$\sum_{\alpha=1}^{M} h_{\beta\alpha}\mu_\alpha = \sum_{\alpha=1}^{M} g_{\beta\alpha}(\mu_\beta - \mu_\alpha) = \kappa_\beta, \quad \beta = 1, \dots, A. \qquad (2.6)$$

Observe that in view of (2.5)

$$0 = \partial_t |\Omega| = \sum_{\beta=1}^{M} \partial_t |\Omega_\beta| = \sum_{\beta=1}^{M} \kappa_\beta - \sum_{\beta,\alpha=1}^{M,M} \mu_\beta g_{\alpha\beta} + \sum_{\beta,\alpha=1}^{M,M} \mu_\alpha g_{\alpha\beta} = \sum_{\beta=1}^{M} \kappa_\beta.$$

Lemma 2.1. *Consider a situation as described at the beginning of Subsec. 2.1.1. If $A < M$ the system* (2.6) *has a unique solution $\mu_1, \dots, \mu_A$. In the case $A = M$*

there is a unique solution $\boldsymbol{\mu} \in \operatorname{span}\{\mathbf{1}_M\}^\perp$ *where* $\mathbf{1}_M = (1, \dots, 1) \in \mathbb{R}^M$ *provided that* $\boldsymbol{\kappa} \cdot \mathbf{1}_M = 0$.

Proof. Let us start with the case $A = M$. Obviously, the vector $\mathbf{1}_M$ then lies in the kernel of $\boldsymbol{H}$. Since $\boldsymbol{H}$ is symmetric it follows that the image of $\mathbb{R}^M$ under $\boldsymbol{H}$ is a subspace of $\operatorname{span}\{\mathbf{1}_M\}^\perp$.

Given $\boldsymbol{\mu} \in \mathbb{R}^M$ a short calculation shows that

$$\boldsymbol{\mu} \cdot \boldsymbol{H}\boldsymbol{\mu} = \frac{1}{2} \sum_{\alpha,\beta=1}^{M} g_{\alpha\beta}(\mu_\alpha - \mu_\beta)^2 \geq 0.$$

Any two line indices $\alpha \neq \beta$ of $\boldsymbol{H}$ are algebraically connected since, by assumption, there is a chain of indices $(\alpha = \eta_1, \eta_2, \dots, \eta_n = \beta)$ such that for each pair $|\Gamma_{\eta_i\eta_{i+1}}| > 0$, whence $g_{\eta_i\eta_{i+1}} > 0$. Therefore, if $\boldsymbol{\mu} \cdot \boldsymbol{H}\boldsymbol{\mu} = 0$ then necessarily $\mu_\alpha = \mu_{\eta_2} = \cdots = \mu_\beta$. Since this holds true for all pairs of indices we have that $\boldsymbol{\mu} \cdot \boldsymbol{H}\boldsymbol{\mu} = 0$ implies $\mu_1 = \cdots = \mu_M$ which is equivalent to $\boldsymbol{\mu} \in \operatorname{span}\{\mathbf{1}_M\}$. The matrix $\boldsymbol{H}$ is therefore strictly positive when restricted to the space $\operatorname{span}\{\mathbf{1}_M\}^\perp$. We conclude that $\boldsymbol{H} : \operatorname{span}\{\mathbf{1}_M\}^\perp \to \operatorname{span}\{\mathbf{1}_M\}^\perp$ is bijective. Since by assumption $\boldsymbol{\kappa} \in \operatorname{span}\{\mathbf{1}_M\}^\perp$, altogether, this determines a unique vector $\boldsymbol{\mu} \in \operatorname{span}\{\mathbf{1}_M\}^\perp$ solving the linear system (2.6).

In the case $A < M$ the volume conserved phases never occupy the whole domain since $\sum_{\alpha=1}^{A} |\Omega_\alpha| = \sum_{\alpha=1}^{A} M_\alpha < |\Omega|$. Consider a maximal set $\mathcal{B} \subset \{1, \dots, A\}$ of algebraically connected indices. By assumption there must always be some hypersurface of non-vanishing surface measure between a conserved phase and a non-conserved phase, i.e., there is a pair of indices $(\alpha, \beta) \in \mathcal{B} \times \{A+1, \dots, M\}$ with $g_{\alpha\beta} > 0$. Therefore, at least one strictly diagonal dominant line exists in the block of the matrix $\boldsymbol{H}$ belonging to the indices $\mathcal{B}$. Hence that block is weakly diagonal dominant. Thanks to the connectedness it is invertible. But since this holds true for all such blocks we obtain that (2.6) is uniquely solvable. □

The Lagrange multipliers may be interpreted as pressures. In the case $A = M$ the pressures are only determined up to a constant. If $A < M$ the pressure in the non-conserved phases are set to zero, and this fixes the pressure in the overall system.

2.1.3. *Decay of energy*

In order to show that the motion described above implies an energy decay we need the following transport identity for a moving surface $\Gamma(t)$ with some smooth surface density γ (cf. the appendix of Ref. 11 for a derivation):

$$\frac{d}{dt}\Big(\int_{\Gamma(t)} \gamma d\mathcal{H}^{d-1}\Big) = \int_{\Gamma(t)} \big(\partial^\circ \gamma - \gamma v \kappa\big) d\mathcal{H}^{d-1} + \int_{\partial\Gamma(t)} \gamma \boldsymbol{v}_{\partial\Gamma} \cdot \boldsymbol{\tau}_\Gamma d\mathcal{H}^{d-2}.$$

Here, v denotes the scalar normal velocity, κ the curvature, $\boldsymbol{v}_{\partial\Gamma}$ the vectorial normal velocity of the boundary $\partial\Gamma$ (considered as a moving surface of dimension $d-2$),

and $\boldsymbol{\tau}_\Gamma$ the external unit normal to Γ on $\partial\Gamma$. The normal-time derivative ∂° in some point $\boldsymbol{x}$ on Γ is defined to be the derivative when following the curve $\boldsymbol{c}(t)$ that is implicitly given as the solution to $\boldsymbol{c}(0) = \boldsymbol{x}$ and $\boldsymbol{c}'(t) = v(\boldsymbol{c}(t))\boldsymbol{\nu}(\boldsymbol{c}(t))$ with the unit normal $\boldsymbol{\nu}$. Moreover we will need the following formula of partial integration on surfaces (e.g., cf. Ref. 5)

$$\int_\Gamma \big(\nabla_s \cdot \boldsymbol{\zeta} + \boldsymbol{\zeta} \cdot \boldsymbol{\nu}\kappa\big) d\mathcal{H}^{d-1} = \int_{\partial\Gamma} \boldsymbol{\zeta} \cdot \boldsymbol{\tau}_\Gamma d\mathcal{H}^{d-2}$$

for a smooth vector field $\boldsymbol{\zeta}$ on Γ, with the same notation as above for the remaining quantities.

Lemma 2.2. *The motion law* (2.1) *together with the boundary conditions* (2.3) *and* (2.4) *and with the system* (2.6) *implies the decay of energy in time, i.e.,*

$$\frac{d}{dt}\mathcal{F}_{SI} \leq 0.$$

Proof. Using $\partial^\circ \boldsymbol{\nu}_{\alpha\beta} = -\nabla_s v_{\alpha\beta}$, $\kappa_{\alpha\beta} = -\nabla_s \cdot \boldsymbol{\nu}_{\alpha\beta}$ (cf. Ref. 5 for these identities), $\boldsymbol{v}_{\partial\Gamma_{\alpha\beta}} \cdot \boldsymbol{\nu}_{\alpha\beta} = v_{\alpha\beta}$, and the motion law (2.1) we see that

$$\begin{aligned}
\frac{d}{dt}\mathcal{F}_{SI} &= \sum_{\alpha<\beta} \int_{\Gamma_{\alpha\beta}} \partial^\circ \gamma_{\alpha\beta}(\boldsymbol{\nu}_{\alpha\beta}) - v_{\alpha\beta}\kappa_{\alpha\beta}\gamma_{\alpha\beta}(\boldsymbol{\nu}_{\alpha\beta}) d\mathcal{H}^{d-1} \\
&\quad + \sum_{\alpha<\beta} \int_{\partial\Gamma_{\alpha\beta}} \gamma_{\alpha\beta}(\boldsymbol{\nu}_{\alpha\beta}) \boldsymbol{v}_{\partial\Gamma_{\alpha\beta}} \cdot \boldsymbol{\tau}_{\alpha\beta} d\mathcal{H}^{d-2} \\
&= \sum_{\alpha<\beta} \int_{\Gamma_{\alpha\beta}} -\nabla_s v_{\alpha\beta} \cdot D\gamma_{\alpha\beta} - v_{\alpha\beta} D\gamma_{\alpha\beta} \cdot \boldsymbol{\nu}_{\alpha\beta}\kappa_{\alpha\beta} d\mathcal{H}^{d-1} \\
&\quad + \sum_{\alpha<\beta} \int_{\partial\Gamma_{\alpha\beta}} \gamma_{\alpha\beta}\boldsymbol{\tau}_{\alpha\beta} \cdot \boldsymbol{v}_{\partial\Gamma_{\alpha\beta}} d\mathcal{H}^{d-2} \\
&= \sum_{\alpha<\beta} \int_{\Gamma_{\alpha\beta}} \nabla_s \cdot D\gamma_{\alpha\beta} \frac{-\nabla_s \cdot D\gamma_{\alpha\beta} + \mu_\beta - \mu_\alpha}{m_{\alpha\beta}} d\mathcal{H}^{d-1} \qquad (2.7) \\
&\quad + \sum_{\alpha<\beta} \int_{\partial\Gamma_{\alpha\beta}} \Big(\gamma_{\alpha\beta}\boldsymbol{\tau}_{\alpha\beta} - \big(D\gamma_{\alpha\beta} \cdot \boldsymbol{\tau}_{\alpha\beta}\big)\boldsymbol{\nu}_{\alpha\beta}\Big) \cdot \boldsymbol{v}_{\partial\Gamma_{\alpha\beta}} d\mathcal{H}^{d-2}. \qquad (2.8)
\end{aligned}$$

For the last identity we applied the above formula of partial integration to the first term.

Let us first consider the boundary part. The set $\partial\Gamma_{\alpha\beta}$ consists of the set $\Gamma_{\alpha\beta,ext}$ and the sets $T_{\alpha\beta\delta}$, $\delta \neq \alpha, \beta$. On $\Gamma_{\alpha\beta,ext}$ the condition (2.4) implies that $\gamma_{\alpha\beta}\boldsymbol{\nu}_{\alpha\beta} + (D\gamma_{\alpha\beta} \cdot \boldsymbol{\tau}_{\alpha\beta})\boldsymbol{\tau}_{\alpha\beta}$ is tangential to $\partial\Omega$ so that its rotation $-(D\gamma_{\alpha\beta} \cdot \boldsymbol{\tau}_{\alpha\beta})\boldsymbol{\nu}_{\alpha\beta} + \gamma_{\alpha\beta}\boldsymbol{\tau}_{\alpha\beta}$ by 90° degree in the plane spanned by $\boldsymbol{\tau}_{\alpha\beta}$ and $\boldsymbol{\nu}_{\alpha\beta}$ is normal to $\partial\Omega$. But since $\Gamma_{\alpha\beta,ext}$ moves along $\partial\Omega$ its vectorial normal velocity is tangential to $\partial\Omega$, hence

$$\Big(\gamma_{\alpha\beta}(\boldsymbol{\nu}_{\alpha\beta})\boldsymbol{\tau}_{\alpha\beta} - \big(D\gamma_{\alpha\beta}(\boldsymbol{\nu}_{\alpha\beta}) \cdot \boldsymbol{\tau}_{\alpha\beta}\big)\boldsymbol{\nu}_{\alpha\beta}\Big) \cdot \boldsymbol{v}_{\partial\Gamma_{\alpha\beta}} = 0 \quad \text{on } \Gamma_{\alpha\beta,ext}.$$

Using the condition on triple lines (2.3) and the fact that the velocities $\boldsymbol{v}_{\partial\Gamma_{\alpha\beta}}$, $\boldsymbol{v}_{\partial\Gamma_{\beta\delta}}$, and $\boldsymbol{v}_{\partial\Gamma_{\delta\alpha}}$ coincide on $T_{\alpha\beta\delta}$ (to avoid a splitting of these sets, the velocities will be denoted by $\boldsymbol{v}_{\alpha\beta\delta}$) we now obtain that the boundary terms in the line (2.8) vanish:

$$\begin{aligned}&\sum_{\alpha<\beta}\int_{\partial\Gamma_{\alpha\beta}}\Big(-\big(D\gamma_{\alpha\beta}(\boldsymbol{\nu}_{\alpha\beta})\cdot\boldsymbol{\tau}_{\alpha\beta}\big)\boldsymbol{\nu}_{\alpha\beta}+\gamma_{\alpha\beta}(\boldsymbol{\nu}_{\alpha\beta})\boldsymbol{\tau}_{\alpha\beta}\Big)\cdot\boldsymbol{v}_{\partial\Gamma_{\alpha\beta}}\\ =&\sum_{\alpha<\beta<\delta}\int_{T_{\alpha\beta\delta}}\Big(\underbrace{\sum_{(i,k)\in\mathcal{A}_{\alpha\beta\delta}}-(D\gamma_{ik}(\boldsymbol{\nu}_{ik})\cdot\boldsymbol{\tau}_{ik})\boldsymbol{\nu}_{ik}+\gamma_{ik}(\boldsymbol{\nu}_{ik})\boldsymbol{\tau}_{ik}}_{=0\text{ by (2.3)}}\Big)\cdot\boldsymbol{v}_{\alpha\beta\delta}.\end{aligned}$$

It remains to consider (2.7). But, using (2.5), it holds that

$$\sum_{\alpha,\beta}(-\mu_\beta+\mu_\alpha)\int_{\Gamma_{\alpha\beta}}\frac{-\nabla_s\cdot(D\gamma_{\alpha\beta}(\boldsymbol{\nu}_{\alpha\beta}))+\mu_\beta-\mu_\alpha}{m_{\alpha\beta}}d\mathcal{H}^{d-1}=0.$$

Hence, noting that $D\gamma_{\beta\alpha}(\boldsymbol{\nu}_{\beta\alpha})=-D\gamma_{\alpha\beta}(\boldsymbol{\nu}_{\alpha\beta})$,

$$(2.7)=-\frac{1}{2}\sum_{\alpha\beta}\int_{\Gamma_{\alpha\beta}}(v_{\alpha\beta})^2\,m_{\alpha\beta}\,d\mathcal{H}^{d-1}\le 0$$

which shows the desired result. □

2.2. *Diffuse interface model*

2.2.1. *Notation and governing equations*

We define the sets $\mathrm{H}\Sigma^M:=\{\boldsymbol{\phi}\in\mathbb{R}^M|\sum_\alpha\phi_\alpha=1\}$, $\Sigma^M:=\{\boldsymbol{\phi}\in\mathrm{H}\Sigma^M|\phi_\alpha\ge 0\,\forall\alpha\}$, and $\mathrm{T}\Sigma^M:=\{\boldsymbol{d}\in\mathbb{R}^M|\sum_\alpha d_\alpha=0\}=\mathrm{span}\{\mathbf{1}_M\}^\perp$. Observe that the tangent space on $\mathrm{H}\Sigma^M$ in some point $\boldsymbol{\phi}\in\mathrm{H}\Sigma$ can naturally be identified with $\mathrm{T}\Sigma^M$.

The gradient potential is a twice differentiable function $a:\mathrm{H}\Sigma^M\times(\mathrm{T}\Sigma^M)^d\to[0,\infty)$ that has the structure

$$a(\boldsymbol{\phi},\nabla\boldsymbol{\phi})=\sum_{\alpha<\beta}A_{\alpha\beta}(\boldsymbol{q}_{\alpha\beta}),\quad \boldsymbol{q}_{\alpha\beta}=\phi_\alpha\nabla\phi_\beta-\phi_\beta\nabla\phi_\alpha,$$

where the functions $A_{\alpha\beta}:\mathbb{R}^d\to(0,\infty)$ are two-homogeneous. The multi-well potential $w:\mathrm{H}\Sigma^M\to[0,\infty]$ has M minima which value zero and which precisely are the corners of Σ^M, i.e., the vectors $e_\alpha=(\delta_{\alpha\beta})_\beta$ with the Kronecker symbol $\delta_{\alpha\beta}$. To allow for different mobilities for the different interfaces we make use of a function

$$\omega:\mathrm{H}\Sigma^M\times(\mathrm{T}\Sigma^M)^d\to(\omega_0,\omega_1)\subset\mathbb{R}$$

with $0<\omega_0\le\omega_1$. We remark that also in the diffuse interface model anisotropic kinetic coefficients can be taken into account[9] since the local orientation of the diffuse interfaces is given in terms of the gradient of $\boldsymbol{\phi}$ on which ω depends (see below).

The evolution of the multi-phase system is defined to be a weighted L^2 gradient flow of the energy (1.4). We consider solutions $\boldsymbol{\phi} = (\phi_1, \ldots, \phi_M) : I \times \Omega \to \mathrm{H}\Sigma^M$ to the system

$$\begin{aligned} \varepsilon\, \omega(\boldsymbol{\phi}, \nabla\boldsymbol{\phi})\, \partial_t \phi_\alpha = {} & \varepsilon \nabla \cdot a_{,\nabla\phi_\alpha}(\boldsymbol{\phi}, \nabla\boldsymbol{\phi}) - \varepsilon a_{,\phi_\alpha}(\boldsymbol{\phi}, \nabla\boldsymbol{\phi}) \\ & - \tfrac{1}{\varepsilon} w_{,\phi_\alpha}(\boldsymbol{\phi}) - f_\alpha(\boldsymbol{\phi}) - \lambda \end{aligned} \tag{2.9}$$

subject to initial values

$$\boldsymbol{\phi}(t=0) = \boldsymbol{\phi}^{(ic)} : \Omega \to \mathrm{H}\Sigma^M, \tag{2.10}$$

with periodic boundary conditions or natural boundary conditions

$$a_{,\nabla\phi_\alpha}(\boldsymbol{\phi}, \nabla\boldsymbol{\phi}) \cdot \boldsymbol{\nu}_{ext} = 0 \text{ on } \partial\Omega, \quad \alpha = 1, \ldots, M, \tag{2.11}$$

and subject to the volume constraints (1.5),

$$\int_\Omega \phi_\alpha(t, \cdot) = M_\alpha = \int_\Omega \boldsymbol{\phi}^{(ic)}, \quad \alpha = 1, \ldots, A, \qquad \forall t \in I. \tag{2.12}$$

For $\partial_t \boldsymbol{\phi} \in \mathrm{T}\Sigma^M$ being fulfilled there is the Lagrange factor

$$\lambda = \frac{1}{M} \sum_{\beta=1}^{M} \varepsilon \nabla \cdot a_{,\nabla\phi_\beta} - \varepsilon a_{,\phi_\beta} - \tfrac{1}{\varepsilon} w_{,\phi_\beta}(\boldsymbol{\phi}) - f_\beta(\boldsymbol{\phi}) \tag{2.13}$$

The forcing terms f_α are chosen in such a way that condition (2.12) is fulfilled. Analogously to (2.2) we set

$$f_\alpha := 0 \quad \text{if } \alpha > A. \tag{2.14}$$

Possible forms of the f_α are discussed in the following subsection.

If the multi-well potential is of obstacle type, i.e., $w(\boldsymbol{\phi}) = \infty$ if $\boldsymbol{\phi} \notin \Sigma^M$, then evolution problem is described by a variational inequality[1]. For almost every $t \in I$ and for all functions $\boldsymbol{\zeta} : \Omega \to \Sigma^M$ a solution $\boldsymbol{\phi}$ satisfies

$$\begin{aligned} 0 \leq \int_\Omega \Big(& \omega(\boldsymbol{\phi}, \nabla\boldsymbol{\phi}) \partial_t \boldsymbol{\phi} \cdot (\boldsymbol{\zeta} - \boldsymbol{\phi}) + a_{,\nabla\boldsymbol{\phi}}(\boldsymbol{\phi}, \nabla\boldsymbol{\phi}) : \nabla\big(\boldsymbol{\zeta} - \boldsymbol{\phi}\big) \\ & + \big(a_{,\boldsymbol{\phi}}(\boldsymbol{\phi}, \nabla\boldsymbol{\phi}) + w_{,\boldsymbol{\phi}}(\boldsymbol{\phi})\big) \cdot (\boldsymbol{\zeta} - \boldsymbol{\phi}) + f(\boldsymbol{\phi}) \cdot (\boldsymbol{\zeta} - \boldsymbol{\phi}) \Big) \end{aligned} \tag{2.15}$$

where the colon operator $: (\mathbb{R}^{n\times m})^2 \to \mathbb{R}$, $A : B = \sum_{i,j} A_{ij} B_{ij}$, appears.

2.2.2. *Choice of the forcing terms*

Let us consider the case of a smooth multi-well potential w. With the abbreviations

$$r_\alpha := \varepsilon \nabla \cdot a_{,\nabla\phi_\alpha} - \varepsilon a_{,\phi_\alpha} - \tfrac{1}{\varepsilon} w_{,\phi_\alpha}, \tag{2.16}$$

$$R_\alpha := \int_\Omega \frac{r_\alpha}{\omega(\boldsymbol{\phi}, \nabla\boldsymbol{\phi})}, \quad \tilde{R}_\alpha := R_\alpha - \frac{1}{M} \sum_{\beta=1}^{M} R_\beta, \quad F_\alpha := \int_\Omega \frac{f_\alpha(\boldsymbol{\phi})}{\omega(\boldsymbol{\phi}, \nabla\boldsymbol{\phi})}$$

we derive from the condition (2.12)

$$0 = \int_\Omega \varepsilon \partial_t \phi_\alpha = \tilde{R}_\alpha - F_\alpha + \frac{1}{M} \sum_{\beta=1}^{A} F_\beta, \quad \alpha = 1, \dots, A. \tag{2.17}$$

In the case $A = 1$ the only equation of (2.17) becomes $0 = \tilde{R}_1 - \frac{M-1}{M} F_1$ which uniquely determines F_1. If $A = M$ we may choose $F_\alpha = R_\alpha$ since then by $\sum_{\alpha=1}^{M} R_\alpha = \sum_{\alpha=1}^{M} F_\alpha$ and the definition of $\tilde{R}_\alpha$ the sums in the conditions (2.17) drop out.

Let us now consider the case $1 < A < M$. Subtracting the identity (2.17) for some $\alpha \in \{1, \dots, A\}$ from the one for some $\beta \in \{1, \dots, A\} \backslash \{\alpha\}$ yields $F_\beta = \tilde{R}_\beta - \tilde{R}_\alpha + F_\alpha$. Replacing the F_β in the identity (2.17) for α then gives after a short calculation

$$F_\alpha = \Big(\tilde{R}_\alpha + \frac{1}{M - A} \sum_{\beta=1}^{A} \tilde{R}_\beta \Big) \quad \text{if } 1 < A < M. \tag{2.18}$$

In the following, $h : \mathbb{R} \to \mathbb{R}$ denotes a monotone increasing interpolation function mapping $[0, 1]$ to $[0, 1]$ such that $h'(p) > 0$ whenever $p \in (0, 1)$. Let us define

$$f_\alpha = \mu_\alpha h'(\phi_\alpha), \quad \alpha = 1, \dots, A.$$

for appropriate values $\mu_\alpha \in \mathbb{R}$. The idea behind this definition is that a possible loss or gain of volume of a phase due to the term $\boldsymbol{r} = (r_1, \dots, r_M)$ is counterbalanced by adding terms to the corresponding phase field variable in the interface-regions to the surrounding phases. The fact that $h'(p) > 0$ whenever $p \in (0, 1)$ is essential for that procedure. The balancing is performed independently of the indices of the neighboring phases.

Setting $H_\alpha := \int_\Omega h'(\phi_\alpha)/\omega(\boldsymbol{\phi}, \nabla \boldsymbol{\phi})$ the discussion above yields that the non-local terms

$$\mu_\alpha = \begin{cases} (M\tilde{R}_1)/((M-1)H_1), & \text{if } A = 1, \\ \big(\tilde{R}_\alpha + \frac{1}{M-A} \sum_{\beta=1}^{A} \tilde{R}_\beta\big)/H_\alpha, & \text{if } 1 < A < M, \\ R_\alpha / H_\alpha, & \text{if } A = M, \end{cases} \tag{2.19}$$

for $\alpha = 1, \dots, A$ are necessary and sufficient in order to guarantee (2.12).

We remark that, in the case of an obstacle multi-well potential w, the above formula for the μ_α needs not to be true (already (2.17) is not true). We found no explicit formula for the forcing terms in that case.

2.2.3. *Remark on the sharp interface asymptotics*

It is possible to relate the diffuse interface model to the sharp interface model as the thickness parameter ε of the diffuse interfaces converges to zero. For this purpose, methods developed in Ref. 16 for the case of two phases and in Ref. 8 for an arbitrary number of phases but without volume constraints were combined.

The method is formal in the sense that suitable asymptotic expansions in ε in the domains of the phases and in the interface-regions are assumed to exist. Matching them yields the equations governing the sharp interface model from the equations of the phase field model. Since the asymptotic analysis did not require essential new ideas and techniques we omit the details.

2.2.4. *Decay of energy*

To investigate whether the energy (1.4) decays we will make use of the abbreviations (2.16), furthermore setting

$$\tilde{r}_\alpha := r_\alpha - \frac{1}{M}\sum_{\beta=1}^{M} r_\beta \quad \text{and} \quad \tilde{f}_\alpha := f_\alpha - \frac{1}{M}\sum_{\beta=1}^{M} f_\beta, \tag{2.20}$$

i.e., $\tilde{\boldsymbol{r}} = (\tilde{r}_1, \dots, \tilde{r}_M)$ and $\tilde{\boldsymbol{f}} = (\tilde{f}_1, \dots, \tilde{f}_M)$ are the projections of $\boldsymbol{r} = (r_1, \dots, r_M)$ and $\boldsymbol{f} = (f_1, \dots, f_M)$ to $T\Sigma^M$ respectively. Observe that if $\alpha > A$ then $f_\alpha = 0$ but, in general, $\tilde{f}_\alpha \neq 0$. Using $\partial_t \boldsymbol{\phi} \in T\Sigma^M$ and (2.9) a short calculation shows that

$$\frac{d}{dt}\mathcal{F}_{GL} = \frac{1}{\varepsilon}\int_\Omega \Big(-\frac{|\tilde{\boldsymbol{r}}|^2}{\omega} + \frac{\tilde{\boldsymbol{r}}\cdot\tilde{\boldsymbol{f}}}{\omega}\Big) \tag{2.21}$$

Let us now assume that the interpolation function h is the identity. Then $f_\alpha = \mu_\alpha$ is constant in space, and the conditions (2.17) give that $\tilde{f}_\alpha \int_\Omega \frac{1}{\omega} = \int_\Omega \frac{\tilde{r}_\alpha}{\omega}$ for the indices $\alpha = 1, \dots, A$. Using that $\tilde{\boldsymbol{f}} \in T\Sigma^M$ is the projection of $\boldsymbol{f} \in \mathbb{R}^M$ and (2.14) we find that

$$\begin{aligned}\tilde{\boldsymbol{f}}\cdot\tilde{\boldsymbol{f}}\int_\Omega \frac{1}{\omega} = \boldsymbol{f}\cdot\tilde{\boldsymbol{f}}\int_\Omega \frac{1}{\omega} &= \sum_{\alpha=1}^{M} f_\alpha \tilde{f}_\alpha \int_\Omega \frac{1}{\omega} = \sum_{\alpha=1}^{A} f_\alpha \tilde{f}_\alpha \int_\Omega \frac{1}{\omega} \\ &= \sum_{\alpha=1}^{A} f_\alpha \int_\Omega \frac{\tilde{r}_\alpha}{\omega} = \sum_{\alpha=1}^{M} f_\alpha \int_\Omega \frac{\tilde{r}_\alpha}{\omega} = \boldsymbol{f}\cdot\int_\Omega \frac{\tilde{\boldsymbol{r}}}{\omega} = \tilde{\boldsymbol{f}}\cdot\int_\Omega \frac{\tilde{\boldsymbol{r}}}{\omega}.\end{aligned}$$

Therefore, adding $0 = \frac{1}{\varepsilon}\int_\Omega \tilde{\boldsymbol{f}}\cdot(\tilde{\boldsymbol{r}} - \tilde{\boldsymbol{f}})/\omega$ to (2.21) yields

$$\frac{d}{dt}\mathcal{F}_{GL} = -\frac{1}{\varepsilon}\int_\Omega \frac{|\tilde{\boldsymbol{r}} - \tilde{\boldsymbol{f}}|^2}{\omega} \leq 0 \quad \text{if } h(r) = r.$$

In the general case of any interpolation function h it is not clear whether this still holds true. But we remark that in the sharp interface limit as $\varepsilon \to 0$ the energy decay property has already been shown in Subsec. 2.1.3.

3. Numerical methods

3.1. *General remarks on the numerical algorithms*

The differential equations or the variational inequality in Subsec. 2.2.1 describing the evolution of the multi-phase system are numerically solved using finite difference methods. The procedure is carefully described in Ref. 9. In space the domain Ω is

supposed to be cubic, and we have a uniform mesh with grid constant Δx. The number of nodes is denoted by $\mathcal{N}$. The value of a field at some node $\boldsymbol{x}_i$, $i \in \{1,\dots,\mathcal{N}\}$, is indicated with a lower index i. In time we use an explicit method, the discrete time step being denoted by Δt. The values of a field at the time $n\Delta t$ is then denoted by an upper index $n \in \{0,\dots,n_{max} := \mathcal{T}/\Delta t\}$. To summarize, we will write

$$\phi_{i\alpha}^n \approx \phi_\alpha(n\Delta t, \boldsymbol{x}_i)$$

where $\boldsymbol{\phi}(t,\boldsymbol{x}) = (\phi_1,\dots,\phi_M)(t,\boldsymbol{x})$ is a solution to the evolution equations.

We assume that every phase involves an interface to another phase and that the grid constant Δx is small enough to resolve all the interface-layers of thickness scaling with ε. In particular, we assume that for every α and every n there is a grid point $\boldsymbol{x}_i$ such that $\phi_{i\alpha}^n \in (0,1)$.

3.2. *Methods for smooth multi-well potentials*

In this subsection the function $w : \mathrm{H}\Sigma^M \to [0,\infty)$ is a smooth function, in applications typically a polynomial. The terms of (2.9) are discretized as described in Ref. 9. In particular, we obtain discrete versions of the terms r_α and $\tilde{r}_\alpha$ defined in (2.16) and (2.20) respectively. Defining initial values on the grid by

$$\phi_{i\alpha}^0 := \phi_\alpha^{(ic)}(\boldsymbol{x}_i) \tag{3.1}$$

the discrete system to solve reads

$$\omega_i^n \frac{\phi_{i\alpha}^{n+1} - \phi_{i\alpha}^n}{\Delta t} = \tilde{r}_{i\alpha}^n - \mu_\alpha^n h'(\phi_{i\alpha}^n) + \frac{1}{M}\sum_{\beta=1}^{A} \mu_\beta^n h'(\phi_{i\beta}^n) \tag{3.2}$$

for $\alpha = 1,\dots,M$, $i = 1,\dots,\mathcal{N}$, and for the time steps $n = 0,\dots,n_{max}-1$.

Also the boundary conditions (2.11), whenever applied, are discretized as in Ref. 9. The volume constraint (2.12) reads

$$(\Delta x)^d \sum_{i=1}^{\mathcal{N}} \phi_{i\alpha}^n = (\Delta x)^d \sum_{i=1}^{\mathcal{N}} \phi_{i\alpha}^0 \quad \forall n. \tag{3.3}$$

In formula (2.19) we already stated how the coefficients μ_α must be such that the volume condition is satisfied. Setting

$$H_\alpha^n := (\Delta x)^d \sum_{i=1}^{\mathcal{N}} \frac{h'(\phi_{i\alpha}^n)}{\omega_i^n}, \quad R_\alpha^n := (\Delta x)^d \sum_{i=1}^{\mathcal{N}} \frac{r_{i\alpha}^n}{\omega_i^n}, \quad \tilde{R}_\alpha^n := R_\alpha^n - \frac{1}{M}\sum_{\beta=1}^{M} R_\beta^n \tag{3.4}$$

we obtain the following version of (2.19) in the discrete setting:

$$\mu_\alpha^n = \begin{cases} (M\tilde{R}_1^n)/((M-1)H_1^n), & \text{if } A = 1, \\ \big(\tilde{R}_\alpha^n + \frac{1}{M-A}\sum_{\beta=1}^{A} \tilde{R}_\beta^n\big)/H_\alpha^n, & \text{if } 1 < A < M, \\ R_\alpha^n/H_\alpha^n, & \text{if } A = M. \end{cases} \tag{3.5}$$

3.3. *Volume equilibration method*

In this subsection we consider multi-well potentials w of obstacle type so that the evolution is described by the variational inequality (2.15).

3.3.1. *General projection method*

A numerical method to solve the variational problem is presented in Ref. 9. It consists of solving a system of equations as for smooth potentials w and, after, a projection of the phase field vectors to the Gibbs simplex Σ^M in each grid point. Thus, given some values μ_α^{n+1}, in every time step we first compute the vectors $\boldsymbol{\phi}_i^{n+1,1/2}$ from the equations

$$\omega_i^n \frac{\phi_{i\alpha}^{n+1,1/2} - \phi_{i\alpha}^n}{\Delta t} = \tilde{r}_{i\alpha}^n - \mu_\alpha^{n+1} h'(\phi_{i\alpha}^n) + \frac{1}{M} \sum_{\beta=1}^{A} \mu_\beta^{n+1} h'(\phi_{i\beta}^n) \tag{3.6}$$

for $\alpha = 1, \ldots, M$ and $i = 1, \ldots, \mathcal{N}$, and after we set

$$\boldsymbol{\phi}_i^{n+1} := \mathcal{P}^M(\boldsymbol{\phi}_i^{n+1,1/2}), \quad i = 1, \ldots, \mathcal{N}, \tag{3.7}$$

where $\mathcal{P}^M : \mathbb{R}^M \to \Sigma^M$ is the projection characterized by

$$(\mathcal{P}^M(\boldsymbol{p}) - \boldsymbol{p}) \cdot (\boldsymbol{v} - \mathcal{P}^M(\boldsymbol{p})) \geq 0 \quad \forall \boldsymbol{v} \in \Sigma^M.$$

Observe that the μ_α appear implicitly in (3.6) in contrast to (3.2). Indeed, since we want that the additional volume constraints (3.3) are satisfied the μ_α^{n+1} will have to be adapted.

In the following we present an iterative ad hoc method to realize the volume constraints without explicitly computing $\boldsymbol{\mu}^{n+1}$.

3.3.2. *Numerical equilibration of the volume change*

In every time step we first take the influence of the $\boldsymbol{r}$-term on the phase field variables into account, i.e., setting $\boldsymbol{\mu}^{n+1} = 0$ in (3.6) we compute for all nodes i

$$\boldsymbol{\phi}_i^{n+1,0} := \mathcal{P}^M\big(\boldsymbol{\phi}_i^n + \frac{\Delta t}{\omega_i^n} \tilde{\boldsymbol{r}}_i^n\big). \tag{3.8}$$

Up to the scaling factor $(\Delta x)^d$, the deviations from the desired volumes are given by $d_\alpha^{n+1,0} := \sum_i (\phi_{i\alpha}^{n+1,0} - \phi_{i\alpha}^0)$, $\alpha = 1, \ldots, A$. We now compute for $\alpha = 1, \ldots, A$

$$\eta_\alpha^{n+1,1} := \begin{cases} \big(d_\alpha^{n+1,0} + \frac{1}{M-A} \sum_{\beta=1}^{A} d_\beta^{n+1,0}\big) \big/ \sum_i h'(\phi_{i\alpha}^n) & \text{if } A < M, \\ d_\alpha^{n+1,0} \big/ \sum_i h'(\phi_{i\alpha}^n) & \text{if } A = M \end{cases}$$

and, setting $\eta_\alpha^{n+1,1} = 0$ if $\alpha > A$, we calculate then for $\alpha = 1, \ldots, M$

$$\phi_{i\alpha}^{n+1,1/2} := \phi_{i\alpha}^{n+1,0} - \eta_\alpha^{n+1,1} h'(\phi_{i\alpha}^n) + \frac{1}{M} \sum_{\beta=1}^{A} \eta_\beta^{n+1,1} h'(\phi_{i\beta}^n).$$

The $\eta_\alpha^{n+1,1}$ are chosen in such a way that the $\boldsymbol{\phi}_i^{n+1,1/2}$ fulfill the volume constraints (3.3) (compare their definition with (3.5)). But since it may be that $\boldsymbol{\phi}_i^{n+1,1/2} \notin \Sigma^M$ in some nodes i we perform a loop over the nodes and compute the vectors $\boldsymbol{\phi}_i^{n+1,1} := \mathcal{P}^M(\boldsymbol{\phi}_i^{n+1,1/2})$. This may destroy again the property that the volume constraints are fulfilled. We therefore iterate the above procedure computing the $d_\alpha^{n+1,1}$, $\eta_\alpha^{n+1,2}$, $\phi_{i\alpha}^{n+1,2}$, $d_\alpha^{n+1,2}$, ... until

$$\max_{1\le\alpha\le A} |d_\alpha^{n+1,k}/(\Delta x)^d| \quad \text{is small enough.}$$

If the function $\omega(\boldsymbol{\phi}, \nabla\boldsymbol{\phi})$ is not constant the motion due to the $\boldsymbol{r}$-term of certain phase interfaces and, eventually, even in certain directions of the phase interfaces is enhanced compared to others. In the above method the equilibration of the volume is performed independently of the type of the phase interface and the local orientation. Indeed, the factors ω_i^n resulting from $\omega(\boldsymbol{\phi}, \nabla\boldsymbol{\phi})$ only appear in (3.8).

Advantages of the above method are the easy implementation due to the logical decoupling of the correction procedure from the update of phase-field values and the (compared to the other methods) lower memory requirements since storing the kinetic coefficients ω_i^n is not necessary, especially when a high number of phases is present.

3.4. *Semi-smooth Newton method*

As in the previous subsection we consider multi-well potentials of obstacle type resulting in a variational inequality of the form (2.15). Again, at every time step we perform (3.6) and (3.7) but now we will present a different way to obtain appropriate forcing terms μ_α^{n+1}. In particular, we address the fact that different kinetic coefficients of the phase interfaces cannot be taken into account by the volume equilibration method presented in the previous subsection.

Consider the function

$$\boldsymbol{f}^{n+1} : \mathbb{R}^A \to \mathbb{R}^A, \quad \boldsymbol{f}^{n+1}(\boldsymbol{\mu}) := (\Delta x)^d \sum_{i=1}^{\mathcal{N}} \left(\phi_{i\alpha}^{n+1}(\boldsymbol{\mu}) - \phi_{i\alpha}^0\right)_{\alpha=1}^A \tag{3.9}$$

for the time step $n \to n+1$ where $\boldsymbol{\phi}_i^{n+1}(\boldsymbol{\mu}) = \mathcal{P}^M(\boldsymbol{\phi}_i^{n+1,1/2}(\boldsymbol{\mu}))$ and the $\phi_{i\alpha}^{n+1,1/2}(\boldsymbol{\mu})$ are computed as in (3.6) with the μ_α^{n+1} replaced by the components of $\boldsymbol{\mu}$. A zero of $\boldsymbol{f}^{n+1}$ means that the volume constraints (3.3) are satisfied. The idea is to use the Newton iteration to compute $\boldsymbol{\mu}^{n+1}$, i.e., we perform an iteration of the form

$$\boldsymbol{\mu}^{n+1,k+1} := \boldsymbol{\mu}^{n+1,k} - (D\boldsymbol{f}^{n+1}(\boldsymbol{\mu}^{n+1,k}))^{-1} \boldsymbol{f}^{n+1}(\boldsymbol{\mu}^{n+1,k}). \tag{3.10}$$

Unfortunately, the function $\boldsymbol{f}^{n+1}$ is not everywhere differentiable because of the projection, whence it may be not clear which value should be assigned to $D\boldsymbol{f}(\boldsymbol{\mu}^{n+1,k})$. But we will show that $\boldsymbol{f}$ is semi-smooth enabling to apply a semi-smooth Newton method. Let us briefly state that $\boldsymbol{f}$ is semi-smooth in $\boldsymbol{\mu}$ if $\boldsymbol{f}$ is locally Lipschitz at

$\boldsymbol{\mu}$ and if for any $\boldsymbol{h} \in \mathbb{R}^A$

$$\lim_{\boldsymbol{B} \in \partial \boldsymbol{f}(\boldsymbol{\mu} + t\boldsymbol{h}'),\, \boldsymbol{h}' \to \boldsymbol{h},\, t \searrow 0} \boldsymbol{B}\boldsymbol{h}' \quad \text{exists.}$$

Here, the generalized derivative $\partial \boldsymbol{f}$ appears. If $D_{\boldsymbol{f}}$ denotes the set on which $\boldsymbol{f}$ is differentiable then it is defined by

$$\partial \boldsymbol{f}(\boldsymbol{\mu}) = \mathrm{co}\Big\{ \lim_{\boldsymbol{\mu}' \to \boldsymbol{\mu},\, \boldsymbol{\mu}' \in D_{\boldsymbol{f}}} D\boldsymbol{f}(\boldsymbol{\mu}') \Big\} \tag{3.11}$$

where $\mathrm{co}(S)$ denotes the convex hull of a set S.

As initial value for the iteration we chose $\boldsymbol{\mu}^{0,0} := 0$ and $\boldsymbol{\mu}^{n+1,0} := \boldsymbol{\mu}^n$ respectively in our simulations.

3.4.1. *Properties of the projection*

In this section we state some properties of the projection $\mathcal{P}^M : \mathbb{R}^M \to \Sigma^M$. By $\mathcal{P}^M$, the space $\mathbb{R}^M$ is divided into a finite number of open polyhedra where $\mathcal{P}^M$ is linear, and on the flat surfaces separating the polyhedra $\mathcal{P}^M$ is continuous but its derivative $D\mathcal{P}^M$ jumps.

Definition 3.1. Let $\boldsymbol{\phi}$ be a regular point of $\mathcal{P}^M$. Define

$$\begin{aligned} \mathcal{R}(\boldsymbol{\phi}) &:= \big\{\beta \in \{1, \dots, M\} | (\mathcal{P}^M(\boldsymbol{\phi}))_\beta \neq 0\big\}, \\ r(\boldsymbol{\phi}) &:= |\mathcal{R}(\boldsymbol{\phi})|, \\ \mathcal{S}(\boldsymbol{\phi}) &:= \{1, \dots, M\} \backslash \mathcal{R}(\boldsymbol{\phi}). \end{aligned}$$

Given a regular point $\boldsymbol{\phi}$ with $\beta_1, \beta_2 \in \mathcal{R}(\boldsymbol{\phi})$ then, close to $\boldsymbol{\phi}$, $\mathcal{P}^M$ is the identity in direction $e_{\beta_1} - e_{\beta_2}$. One can conclude the following lemma:

Lemma 3.1. *Let $\boldsymbol{\phi}$ be a regular point of $\mathcal{P}^M$ and let $\mathcal{R}(\boldsymbol{\phi}) = \{\beta_k\}_{k=1}^{r(\boldsymbol{\phi})}$. The derivative of $\mathcal{P}^M$ in $\boldsymbol{\phi}$ in direction $d \in \mathbb{R}^M$ is*

$$D\mathcal{P}^M(\boldsymbol{\phi})d = \text{ projection of } d \text{ to span}\{e_{\beta_1} - e_{\beta_2}, \dots, e_{\beta_{r(\boldsymbol{\phi})-1}} - e_{\beta_{r(\boldsymbol{\phi})}}\}. \tag{3.12}$$

In particular, if $d = e_\alpha = (\delta_{\alpha\beta})_{\beta=1}^M$ with the Kronecker symbols $\delta_{\alpha\beta}$ and if $\alpha \in \mathcal{R}(\boldsymbol{\phi})$ then

$$D\mathcal{P}^M(\boldsymbol{\phi}) \cdot e_\alpha = \begin{cases} 0, & \text{if } \delta \in \mathcal{S}(\boldsymbol{\phi}), \\ \frac{r(\boldsymbol{\phi})-1}{r(\boldsymbol{\phi})}, & \text{if } \delta = \alpha, \\ \frac{-1}{r(\boldsymbol{\phi})}, & \text{if } \delta \in \mathcal{R}(\boldsymbol{\phi}) \backslash \{\alpha\}. \end{cases} \tag{3.13}$$

Let now $\boldsymbol{\phi} \in \mathbb{R}^M$ be a point where $\mathcal{P}^M$ is not regular. Then there is a closed ball $B_\delta(\boldsymbol{\phi})$ with sufficiently small radius $\delta > 0$ around $\boldsymbol{\phi}$ such that the cut with each of the adjacent polyhedra is a ball segment with tip in $\boldsymbol{\phi}$. More precisely, given any adjacent polyhedron H and any point $\boldsymbol{h} \in (B_\delta(\boldsymbol{\phi}) \cap H) \backslash \{\boldsymbol{\phi}\}$ then also the set $\{\boldsymbol{\phi} + r\frac{\boldsymbol{h}-\boldsymbol{\phi}}{\|\boldsymbol{h}-\boldsymbol{\phi}\|} | r \in (0, \delta)\}$ belongs to $B_\delta(\boldsymbol{\phi}) \cap H$. Therefore, given some $\boldsymbol{h} \in \mathrm{T}\Sigma^M$ with $\|\boldsymbol{h}\| < \delta$, the linearity of $\mathcal{P}^M$ in every polyhedron implies that the directional

derivatives in direction $\boldsymbol{h}$ in the points $\boldsymbol{\phi}$ and $\boldsymbol{\phi}+\boldsymbol{h}$ agree. But this means that the criterion (v) of Theorem 2.3 in Ref. 15 is fulfilled. As a conclusion of that theorem we get

Lemma 3.2. *The projection $\mathcal{P}^M : \mathbb{R}^M \to \Sigma^M$ is semi-smooth.*

The generalized derivative $\partial\mathcal{P}^M$ of the projection is defined as in (3.11). If $\boldsymbol{\phi}$ is a regular point we have $\partial\mathcal{P}^M(\boldsymbol{\phi}) = \{D\mathcal{P}^M(\boldsymbol{\phi})\}$. In the other case $\partial\mathcal{P}^M(\boldsymbol{\phi})$ is the convex hull of a finite number of matrices, namely, the values of $D\mathcal{P}^M$ in the polyhedra adjacent to $\boldsymbol{\phi}$.

3.4.2. *Local convergence*

Assume that there is a solution $\boldsymbol{\mu}^{n+1}$ to the equation $\boldsymbol{f}^{n+1}(\boldsymbol{\mu}) = 0$. Theorem 3.2 of Ref. 15 yields local convergence of the Newton iteration to $\boldsymbol{\mu}^{n+1}$ if we show that $\boldsymbol{f}^{n+1}$ is semi-smooth and locally Lipschitz, and that the elements belonging to $\partial\boldsymbol{f}^{n+1}(\boldsymbol{\mu})$ for all $\boldsymbol{\mu}$ close to $\boldsymbol{\mu}^{n+1}$ are regular matrices. Since $\mathcal{P}^M$ is Lipschitz and semi-smooth and since $\boldsymbol{\phi}_i^{n+1,1/2}(\boldsymbol{\mu})$ is linear in $\boldsymbol{\mu}$ the first and second necessary property of $\boldsymbol{f}^{n+1}$ follow immediately.

Lemma 3.3. *Let $\boldsymbol{\mu}^{n+1}$ be a solution to the equation $\boldsymbol{f}^{n+1}(\boldsymbol{\mu}) = 0$ and assume that $A < M$. For all $\boldsymbol{\mu}$ in a small neighborhood of $\boldsymbol{\mu}^{n+1}$ any $\boldsymbol{B} = (b_{\alpha\beta})_{\alpha,\beta=1}^{A} \in -\partial\boldsymbol{f}^{n+1}(\boldsymbol{\mu})$ can be divided into blocks which are M-matrices.*

For the definition of and facts on M-matrices we refer to standard literature on numerical methods for partial differential equations. By the sum condition (1.3) the omitted case $A = M$ is equivalent to the case $A = M - 1$.

Proof. Let $\boldsymbol{\mu}^{n+1}$ and $\boldsymbol{B}$ be given as in the assertion. The chain rule leads to

$$\partial\boldsymbol{f}^{n+1}(\boldsymbol{\mu}) = \Big(\partial\mathcal{P}_\delta^M(\boldsymbol{\phi}_i^{n+1,1/2}(\boldsymbol{\mu}))D\boldsymbol{\phi}_i^{n+1,1/2}(\boldsymbol{\mu})\Big)_{\delta=1}^{A}$$

where we have that $\partial_{\mu_\alpha}\boldsymbol{\phi}_i^{n+1,1/2}(\boldsymbol{\mu}) = -\frac{\Delta t}{\omega_i^n}h'(\phi_{i\alpha}^n)(e_\alpha - \frac{1}{M}\mathbf{1}_M)$. Observe that $\partial\mathcal{P}^M(\boldsymbol{\phi})\mathbf{1}_M = 0$ for all $\boldsymbol{\phi}$ since $\mathbf{1}_M \perp \Sigma^M$.

Let us first consider the case that $\boldsymbol{\phi}_i^{n+1,1/2}(\boldsymbol{\mu})$ is a regular point. By definition $\mathcal{R}(\boldsymbol{\phi}_i^{n+1,1/2}) = \mathcal{R}(\boldsymbol{\phi}_i^{n+1,1})$, $r(\boldsymbol{\phi}_i^{n+1,1/2}) = r(\boldsymbol{\phi}_i^{n+1,1})$, and $\mathcal{S}(\boldsymbol{\phi}_i^{n+1,1/2}) = \mathcal{S}(\boldsymbol{\phi}_i^{n+1,1})$. If $\alpha \in \mathcal{S}(\boldsymbol{\phi}_i^{n+1,1})$ then we have by (3.12)

$$\big(D\mathcal{P}^M(\boldsymbol{\phi}_i^{n+1,1/2})e_\alpha\big)_\delta = 0 \quad \forall\delta \in \{1,\dots,M\}. \tag{3.14}$$

If $\alpha \in \mathcal{R}(\boldsymbol{\phi}_i^{n+1,1})$ then with (3.13)

$$\big(D\mathcal{P}^M(\boldsymbol{\phi}_i^{n+1,1/2})e_\alpha\big)_\delta = \begin{cases} 0 & \text{if } \delta \in \mathcal{S}(\boldsymbol{\phi}_i^{n+1,1}), \\ \frac{r(\boldsymbol{\phi}_i^{n+1,1})-1}{r(\boldsymbol{\phi}_i^{n+1,1})} & \text{if } \delta = \alpha, \\ \frac{-1}{r(\boldsymbol{\phi}_i^{n+1,1})} & \text{if } \delta \in \mathcal{R}(\boldsymbol{\phi}_i^{n+1,1})\backslash\{\alpha\}. \end{cases} \tag{3.15}$$

This leads to

$$\begin{aligned}\big(D\mathcal{P}^M(\boldsymbol{\phi}_i^{n+1,1/2}(\boldsymbol{\mu}))\partial_{\mu_\alpha}\boldsymbol{\phi}_i^{n+1,1/2}(\boldsymbol{\mu})\big)_\delta \\ = -\frac{\Delta t}{\omega_i^n}h'(\phi_{i\alpha}^n)\begin{cases}0 & \text{if } \delta\in\mathcal{S}(\boldsymbol{\phi}_i^{n+1,1}(\boldsymbol{\mu})),\\ \frac{r(\boldsymbol{\phi}_i^{n+1,1}(\boldsymbol{\mu}))-1}{r(\boldsymbol{\phi}_i^{n+1,1}(\boldsymbol{\mu}))} & \text{if } \delta=\alpha,\\ \frac{-1}{r(\boldsymbol{\phi}_i^{n+1,1}(\boldsymbol{\mu}))} & \text{if } \delta\in\mathcal{R}(\boldsymbol{\phi}_i^{n+1,1}(\boldsymbol{\mu}))\backslash\{\alpha\}.\end{cases}\end{aligned} \tag{3.16}$$

In the other case, any element $\boldsymbol{P}=(p_{\delta\alpha})_{\delta,\alpha}^M\in\partial\mathcal{P}^M(\boldsymbol{\phi}_i^{n+1,1/2}(\boldsymbol{\mu}))$ is a convex combination of projections (compare the remark below Lemma 3.2) so that $p_{\delta\alpha}$ is a convex combination of identities as in (3.15). For the following, we may restrict our attention to regular points. It is easy to see that the subsequent argumentation is still valid in the case of convex combinations.

The factors $-\frac{\Delta t}{\omega_i^n}h'(\phi_{i\alpha}^n)$ are always non-positive. Therefore, the contribution of node i to the diagonal elements $b_{\alpha\alpha}$ are always non-positive while the other contributions on non-diagonal elements are always non-negative.

By the assumption stated at the end of Subsec. 3.1 there is some node i such that $\phi_{i\alpha}^{n+1}(\boldsymbol{\mu}^{n+1})\in(0,1)$, whence $h'(\phi_{i\alpha}^{n+1}(\boldsymbol{\mu}^{n+1}))>0$. From the sum condition $\sum_\alpha\phi_{i\alpha}^{n+1}=1$ we see that there needs to be another index δ with $\phi_{i\delta}^{n+1}(\boldsymbol{\mu}^{n+1})\in(0,1)$. By the Lipschitz continuity of $\mathcal{P}^M$ we conclude that $r(\boldsymbol{\phi}_i^{n+1,1}(\boldsymbol{\mu}))\geq 2$ for all $\boldsymbol{\mu}$ in a small neighborhood of $\boldsymbol{\mu}^{n+1}$. In view of the contribution (3.16) of node i to the column α of $\boldsymbol{B}$ this implies that the diagonal entries of $\boldsymbol{B}$ are strictly negative. Moreover, the contribution to the entry $b_{\delta\alpha}$ means that the lines δ and α in $\boldsymbol{B}$ are algebraically connected. The maximal connected blocks of $\boldsymbol{B}$ are therefore irreducible. For shorter presentation, we now assume that $\boldsymbol{B}$ in total is irreducible.

We will show the weak column sum criterion from which we can conclude that $\boldsymbol{B}$ is an M-matrix. Let the line index δ run from 1 to M in (3.16). The number of entries set to $\frac{\Delta t}{\omega_i^n}h'(\phi_{i\alpha}^n)/r(\boldsymbol{\phi}_i^{n+1,1}(\boldsymbol{\mu}))$ is just $r(\boldsymbol{\phi}_i^{n+1,1}(\boldsymbol{\mu}))-1$. Summing up the entries over δ we obtain zero. We conclude that for every $\alpha\in\{1,\dots,A\}$

$$|b_{\alpha\alpha}|\geq\sum_{\substack{1\leq\delta\leq A\\ \delta\neq\alpha}}|b_{\delta\alpha}|. \tag{3.17}$$

It remains to show that this inequality becomes strict for some index α. But since $A<M$ there is some phase α with some transition region to some non-conserved phase $\beta>A$, i.e., there is some node i with

$$\big(D\mathcal{P}^M(\boldsymbol{\phi}_i^{n+1,1/2}(\boldsymbol{\mu}))\partial_{\mu_\alpha}\boldsymbol{\phi}_i^{n+1,1/2}(\boldsymbol{\mu})\big)_\beta=\frac{\Delta t}{\omega_i^n}h'(\phi_{i\alpha}^n)/r(\boldsymbol{\phi}_i^{n+1,1}(\boldsymbol{\mu}))<0.$$

This contribution is missing on the right hand side of (3.17) so that the inequality becomes strict for that α. □

Altogether, thanks to the previous lemma and the facts on $\mathcal{P}^M$ stated in Subsec. 3.4.1 the function $\boldsymbol{f}$ defined in (3.9) is semi-smooth. With Theorem 3.2 of Ref. 15 we obtain the following result:

Theorem 3.1. *Replacing* $D\boldsymbol{f}(\boldsymbol{\mu}^{n+1,k})$ *by some matrix* $\boldsymbol{B} \in \partial \boldsymbol{f}(\boldsymbol{\mu}^{n+1,k})$ *the Newton iteration* (3.10) *is well defined and locally superlinearly convergent.*

3.4.3. *Remarks on the numerical implementation*

In the case that $\boldsymbol{\mu}^{n+1,k}$ is not a regular point of $\boldsymbol{f}$ or, equivalently, the corresponding iterative $\boldsymbol{\phi}_i^{n+1,k+1/2}(\boldsymbol{\mu}^{n+1,k})$ computed from (3.6) with $\boldsymbol{\mu}^{n+1}$ replaced by $\boldsymbol{\mu}^{n+1,k}$, is not a regular point of $\mathcal{P}^M$, we make the cheapest choice by extending Def. 3.1 and formula (3.12) to that case, i.e., we set $D\boldsymbol{f}(\boldsymbol{\mu}^{n+1,k}) := (\sum_{i=1}^{\mathcal{N}} f_{\delta\alpha,i})_{\delta,\alpha=1}^{A}$, where $f_{\delta\alpha,i} := 0$ in the case $\alpha \in \mathcal{S}(\boldsymbol{\phi}_i^{n+1,k+1}(\boldsymbol{\mu}^{n+1,k}))$, and in the case $\alpha \in \mathcal{R}(\boldsymbol{\phi}_i^{n+1,k+1}(\boldsymbol{\mu}^{n+1,k}))$

$$f_{\delta\alpha,i} := -\frac{\Delta t}{\omega_i^n} h'(\phi_{i\alpha}^n) \begin{cases} 0 & \text{if } \delta \in \mathcal{S}(\boldsymbol{\phi}_i^{n+1,k+1}(\boldsymbol{\mu}^{n+1,k})), \\ \frac{r-1}{r} & \text{if } \delta = \alpha, \\ \frac{-1}{r} & \text{if } \delta \in \mathcal{R}(\boldsymbol{\phi}_i^{n+1,k+1}(\boldsymbol{\mu}^{n+1,k}))\backslash\{\alpha\}. \end{cases}$$

with $r := r(\boldsymbol{\phi}_i^{n+1,k+1}(\boldsymbol{\mu}^{n+1,k}))$.

Observe that the right hand side only depends on the projected points $\boldsymbol{\phi}_i^{n+1,k+1} = \mathcal{P}^M(\boldsymbol{\phi}_i^{n+1,k+1/2})$. By that computation also the index sets $\mathcal{R}(\boldsymbol{\phi}_i^{n+1,k+1})$, $\mathcal{S}(\boldsymbol{\phi}_i^{n+1,k+1})$, and the numbers $r(\boldsymbol{\phi}_i^{n+1,k+1})$ are known. Moreover, the values $\frac{\Delta t}{\omega_i^n}$ and $h'(\phi_{i\alpha}^n)$ have been used earlier. That's why the computational effort to assemble the matrix $D\boldsymbol{f}^{n+1}(\boldsymbol{\mu}^{n+1,k})$ is of the order $O(\mathcal{N})$ and, hence, optimal.

In order to solve the linear system (3.10) we used a standard QR decomposition algorithm. An iterative method seemed to be inappropriate because in the considered applications the number A of conserved phases was always small (four or lower).

4. Applications

4.1. *General remarks on the parameter choices*

If not otherwise stated we made the following choices for the parameters and potentials in the simulations presented in the subsequent sections.

The simulations were carried out on regular grids with a spacing of $\Delta x = 0.02$ and a diffuse interface parameter of $\varepsilon = 0.06$. The time step width Δt of the explicit scheme was $4 \cdot 10^{-5}$ for 2D and $3 \cdot 10^{-5}$ for 3D simulations.

To initialize the phase fields we first considered values in $\{0, 1\}$, i.e., we had jump discontinuities and sharp interfaces between the phases. A smoothing operation was then applied that preserved the initialized volumes $(\Delta x)^d \sum_i \phi_{i\alpha}$. It essentially consisted in performing some time steps of a discretized heat equation for the ϕ_α.

We used the gradient potential

$$a(\boldsymbol{\phi}, \nabla\boldsymbol{\phi}) = \sum_{\alpha<\beta} g_{\alpha\beta} |\phi_\alpha \nabla\phi_\beta - \phi_\beta \nabla\phi_\alpha|^2$$

and the smooth multi-well potential

$$w(\boldsymbol{\phi}) = \sum_{\alpha<\beta} 9 g_{\alpha\beta} \phi_\alpha^2 \phi_\beta^2 + \sum_{\alpha<\beta<\delta} g_{\alpha\beta\delta} \phi_\alpha^2 \phi_\beta^2 \phi_\delta^2 \tag{4.1}$$

with $g_{\alpha\beta} = 1$ and $g_{\alpha\beta\delta} = 6$. As discussed in Ref. 9 and 7 the above potentials correspond to isotropic surface energies $\gamma_{\alpha\beta}(\boldsymbol{\nu}) = g_{\alpha\beta}$. The kinetic coefficients are set to one, $m_{\alpha\beta} = 1$, and to realize this we always made the choice $\omega(\boldsymbol{\phi}, \nabla\boldsymbol{\phi}) = 1$.

Sometimes we used the obstacle multi-well potential

$$w(\boldsymbol{\phi}) = \begin{cases} \frac{16}{\pi^2} \sum_{\alpha<\beta} g_{\alpha\beta} \phi_\alpha \phi_\beta + \sum_{\alpha<\beta<\delta} g_{\alpha\beta\delta} \phi_\alpha \phi_\beta \phi_\delta, & \phi \in \Sigma^M, \\ \infty, & \phi \notin \Sigma^M. \end{cases} \tag{4.2}$$

in combination with one of the iterative schemes. Then we set the tolerance rate to 10^{-6} for the fraction $\sum_i (\phi_{i\alpha}^n - \phi_{i\alpha}^0) / \sum_i \phi_{i\alpha}^0$ of the volume difference and the initial volume, $\alpha = 1, \ldots, A$. We here already remark that for both methods, the volume equilibration method (Subsec. 3.3) and the semi-smooth Newton method (Subsec. 3.4), usually one iteration step was necessary in each time step to achieve that tolerance. Moreover, the computational time was comparable for both methods.

In the figures presented in the following the level sets $\phi_\alpha = 0.5$ are shown for some or all of the indices $\alpha \in \{1, \ldots, M\}$.

4.2. *Survival of the fattest*

Situations where the solution to the sharp interface model is explicitly known or can easily be computed provide appropriate tests for the numerical methods presented in the Subsec. 3.2, 3.3, and 3.4. Exemplary, let us consider two phases (1 and 2) of conserved volume which are initially arranged as follows. Phase 2 occupies a domain consisting of two separate balls surrounded by a connected domain of phase 1. With $\gamma_{12} = 1$ and $\omega_{12} = 1$ in (2.1) the boundaries of the balls move according to an isotropic curvature flow, modified by the additional terms in the evolution equation ensuring the volume conservation. In particular, the balls maintain their shape, and the evolution can be described in terms of their radii $r_1(t)$ and $r_2(t)$. The motion law (2.1) implies that these functions satisfy the ordinary differential equations

$$\dot{r}_1 = -\frac{1}{r_1} + \frac{2}{r_1 + r_2}, \quad \dot{r}_2 = -\frac{1}{r_2} + \frac{2}{r_1 + r_2}, \tag{4.3}$$

until one of the balls vanishes.

Solving (4.3) numerically with an explicit Runge-Kutta method (see below for initial radii) yields an approximation of the surface energy evolution $E_{cont}(t) := 2\pi(r_1(t) + r_2(t))$ that can be compared with the discrete version of (1.4)

$$E_{dis}(n\,\Delta t) := (\Delta x)^d \sum_{i=1}^{\mathcal{N}} \Big(\varepsilon a(\boldsymbol{\phi}_i^n, (\nabla_{\Delta x} \boldsymbol{\phi}^n)_i) + \frac{1}{\varepsilon} w(\boldsymbol{\phi}_i^n) \Big) \tag{4.4}$$

where $(\nabla_{\Delta x}\boldsymbol{\phi}^n)_i = (\boldsymbol{\phi}^n_{i+1} - \boldsymbol{\phi}^n_{i-1})/2\,\Delta x$ stands for the central difference operator and the $\{\boldsymbol{\phi}^n_i\}_i$ are solutions obtained from the presented algorithms.

The simulation domain $(0,4)\times(0,2)$ was chosen and the balls were centered in $(1,1)$ and $(3,1)$ with initial radii $r_1(0) = 0.4$ and $r_2(0) = 0.6$. Only one smoothing step was performed but the discontinuities were quickly smeared out during the first time steps, and interface-layers with a thickness of the order ε appeared. We performed simulations for $\varepsilon \in \{\sqrt{2}/10, 1/10, 1/(\sqrt{2}\cdot 10)\}$ with grid constants $\Delta x \in \{0.02, 0.01\}$ and time steps $\Delta t = 4\cdot 10^{-5}$ and 10^{-5} respectively.

The evolution for the smooth multi-well potential (4.1) and for the obstacle potential (4.2) with the iterative procedures turned out to be similar. Fig. 1 indicates that the energy (4.4) converges as $\varepsilon \to 0$, here shown for the obstacle potential in combination with the Newton method. Similar behaviors were found when applying the other methods.

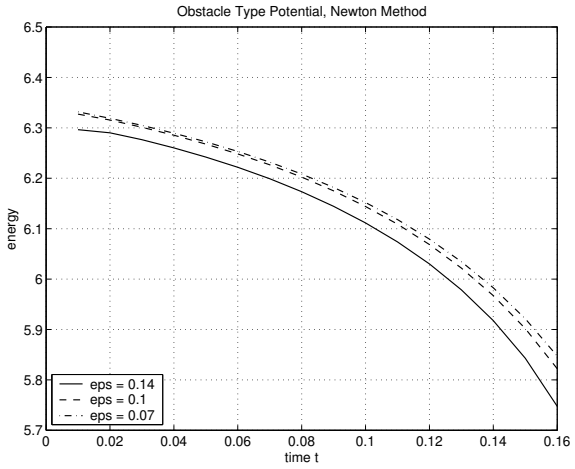

Fig. 1. Convergence of the system energy with decreasing ε, simulation results for $\Delta x = 0.01$.

The simulation for $\varepsilon = 0.1$ and $\Delta x = 0.01$ was compared to the solution to the sharp interface model, whose evolution started at time $t = 0.01$ when nice smooth diffuse interface layers had formed from the initial jumps. The initial values for (4.3) were set as follows. We measured the energy (4.4) from the phase field simulations at $t = 0.01$ separately on the two domains $(0,2)\times(0,2)$ and $(2,4)\times(0,2)$, each of them containing one of the two balls. Dividing each energy by 2π we got the radii $\bar{r}_1 \approx 0.388, \bar{r}_2 \approx 0.598$ of two circles of the same total surface energy in the sharp interface model, which were used as initial values at time $t = 0.01$.

Fig. 2 shows a good agreement in the energy evolution of the sharp interface model and the phase field model (Newton method). A clear deviation from the sharp interface dynamics only arises at time of about $t = 0.2$, when the ball of phase 2

with smaller initial radius reaches a radius in the range of the interface width ε.

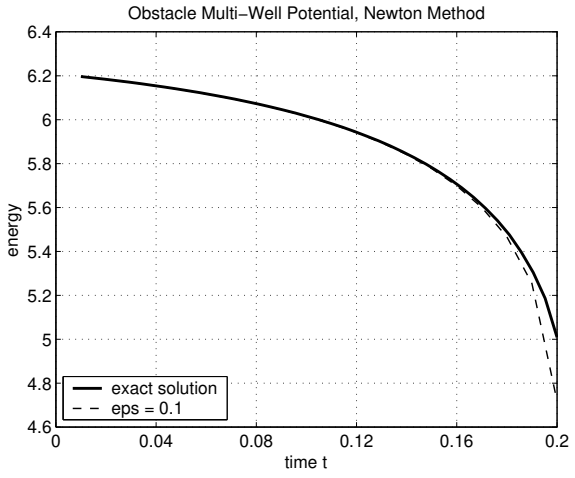

Fig. 2. Comparing the evolution of the energy for the sharp interface model and the phase field model.

4.3. *Bubbles*

4.3.1. *Three bubbles in 2D with volume conservation*

In a domain of 200×200 grid points three bubbles with square shape and equal area of 80×80 grid points were initially set as shown in Fig. 3**a**. The bubbles were represented by 3 different phase-field parameters embedded in a fourth matrix phase. Fig. 3 shows the evolution of the interfaces. A configuration of three identical circular segments with planar intersections meeting at an angle of 120° is finally reached (chart **c**) in accordance with condition (2.3).

4.3.2. *Three bubbles in 2D, only two of them with volume conservation*

We studied the case of three adjacent bubbles where only two of them were subject to a volume conservation. The equilibration method in Subsec. 3.3 with the obstacle potential (4.2) with $g_{\alpha\beta\delta} = 6$ was chosen. The initial configuration is shown in Fig. 4**a** where the squares have a size of 61×61, the rectangle of 61×122, and the whole domain of 200×200 grid points.

Due to its convexity and interface curvature the bubble with non-preserved phase volume shrinks and disappears. In Fig. 4**d** the final configuration of a double bubble is reached which consists of portions of three intersecting spheres. This configuration was shown to be the minimal energy surface in $\mathbb{R}^2$ (see Ref. 6) and $\mathbb{R}^3$ (see Ref. 13).

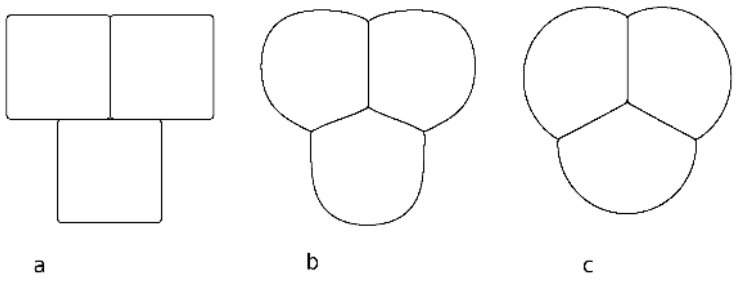

Fig. 3. Evolution of a system of three bubbles with preserved volume. The pictures represent the shape at times 0.0, 0.0825, and 1.185 (**a** - **c**)

The curvature of the partition sphere follows the relation[14]

$$\frac{1}{R} = \frac{1}{r_2} - \frac{1}{r_1}, \tag{4.5}$$

with R denoting the radius of the intersection circular segment and r_1 and r_2 the radii of the bubbles. We extracted radii $\tilde{r}_1$, $\tilde{r}_2$, and $\tilde{R}$ from the simulation data by fitting circles to the $\phi = 0.5$ contour lines, $\tilde{r}_1$ being the radius of the greater bubble. Replacing r_1 and r_2 in (4.5) by $\tilde{r}_1$ and $\tilde{r}_2$ we get an expected radius $\tilde{R}'$ for the intersection circular. It turned out that the fraction $\tilde{R}/\tilde{r}_1 = 3.16$ was a little bit to small compared to the expected fraction $\tilde{R}'/\tilde{r}_1 = 3.31$ but we remark that the problem of fitting spheres with big radii is ill-conditioned.

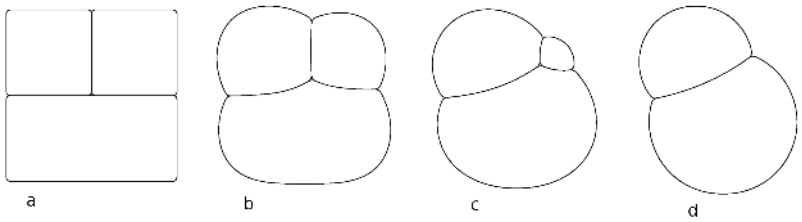

Fig. 4. Evolution of a system of three bubbles, one of them with non-preserved volume (upper right one at **a**). The pictures represent the shape at times 0.0, 0.105, 0.3075, and 1.50 (**a** - **d**)

Additionally, we compared the above used obstacle potential with the volume correction method of Subsec. 3.2 for the smooth potential[7]

$$w(\boldsymbol{\phi}) = \sum_{\alpha<\beta} 9\phi_\alpha^2\phi_\beta^2\big(1 + 8\sum_{\delta\neq\alpha,\beta}\phi_\delta\big) + \sum_{\alpha<\beta<\delta} 6\phi_\alpha^2\phi_\beta^2\phi_\delta^2.$$

Here, the initial configuration corresponds to the situation in Fig. 3**a**, the upper right phase not being due to volume conservation. The bubble contours after simulation

time $t = 0.353$ and 0.555 are depicted in Fig. 5. Only for intermediate states small deviations in the shape can be seen, especially for the boundary of the vanishing grain in chart on the left in Fig. 5. The resulting shapes on the right in Fig. 5 are almost indistinguishable for both methods.

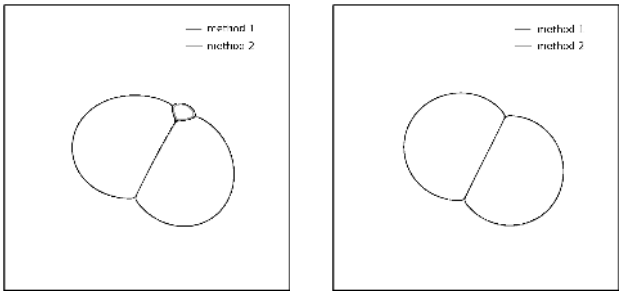

Fig. 5. Comparison of volume preservation methods for a smooth (black line) and non-smooth potential (gray line). Starting with the configuration of Fig. 3**a** with only two bubbles due to volume constraints, the results are shown at time t = 0.3525 (left) and 0.555 (right).

Concerning the computational efficiency, the iterative procedure has a slight drawback to the direct method for the smooth potential during the first time steps which is associated with a strong rearrangement of phase volume (5 to 10 iterations were necessary to achieve a tolerance ratio of 10^{-6}). But this was compensated during the long run, where often a single iteration step was sufficient.

4.3.3. *Double bubbles in 3D*

The simulations in 3D were started with two adjoining bubbles with cuboid geometry on a domain of $150 \times 75 \times 75$ grid points and were terminated after reaching a stationary shape. The final configurations for three different bubble volume ratios of 1.0, 0.484 and 0.252 (**a** - **c**, from left to right) and intersection profiles are shown in Fig. 6.

The evolution of a more exotic double bubble is shown in Fig. 7, **a** - **c**. The grid size is $70 \times 90 \times 90$. The disk shaped first phase has a radius of 60 grid points and width of 16 grid points. The second phase, wrapped around the disk like a tire around a wheel rim, has also a width of 16 grid points and a thickness of 7 grid points. The simulation results in a stationary torus/dumbbell configuration (chart **c**). The volume relation of the torus/dumbbell bubbles is 0.54. After choosing a greater fraction (e.g. 0.91) by thickening the second phase the torus bubble merges to a simply connected shape cutting the dumbbell into two parts.

We studied the stability of the torus/dumbbell. The simulation was restarted using the configuration of Fig. 7 **c** as initial state. A small amount of Gaussian distributed noise in the diffuse interface region of each phase field parameter was

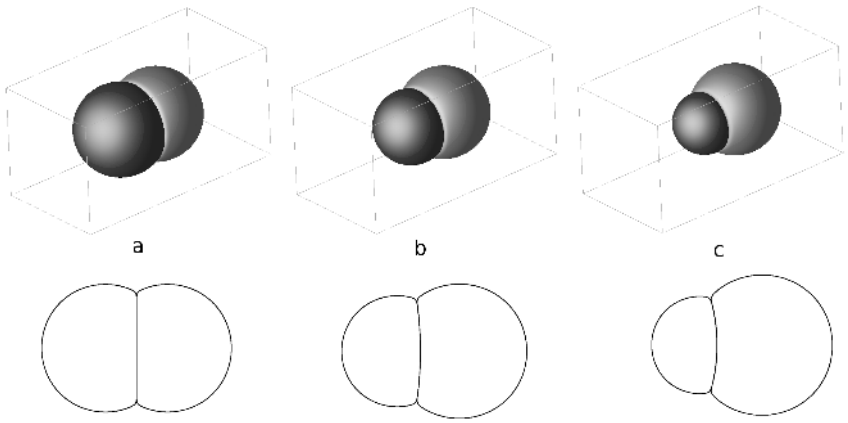

Fig. 6. Three different double bubble configurations with intersection profiles through the symmetry axis.

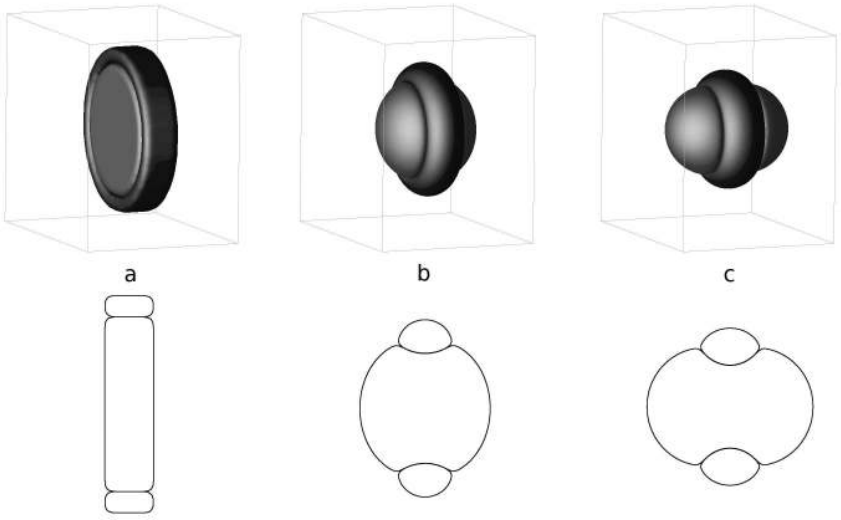

Fig. 7. Evolution of the torus-dumbbell configuration.

added to perturb the system. This resulted always in a thinning of the toroidal ring at one point and a swelling at the diametrical opposed side (see Fig. 8) until the ring tore apart and formed a simple double bubble as in Fig. 6. The torus was in no case found to be stripped off the dumbbell in direction of the symmetry axis, as one might intuitively assume. We remark that in such situations the phase field approach is advantageous compared to sharp interface methods (e.g., cf. Ref. 2)

since topological changes of the phase arrangement are captured in a natural way.

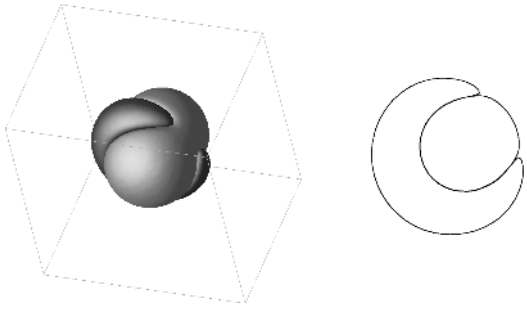

Fig. 8. Effect of perturbation with interfacial noise for the torus/dumbbell system of Fig. 7 **c**. A snapshot after deformation and tearing of the torus is shown.

4.4. *Tessellations*

An intuitive application of volume preservation in the phase-field framework is the study of tessellations. A tessellation is a periodic arrangement (a periodic tiling) of polygons in 2D or polyhedra in 3D which fill the plane (or space) completely. Our goal is to obtain tessellations by solving the following

> **Tessellation Problem:** Given a rectangular or cuboidal periodicity cell in 2D or 3D, respectively, find a partition into a fixed number of sub-domains with given area/volume such that the surface energy of the type (1.1) is minimal.

The idea is to define an initial space partitioning and to let the system relax to an energetically favorable state. Contrary to the bubble simulations discussed before, no additional surrounding 'matrix' phase is present to embed the geometrical objects. It is necessary to state that the dimensions of the periodic simulation domain influence the resulting structure. The simulation parameters of Subsec. 4.1 were used except a higher interface width by setting $\varepsilon = 0.1$.

4.4.1. *Tessellations in 2D*

On a domain of 200×200 grid points 4 phases were initially filled in adjacent sectors of equal area (see Fig. 9**a**). Keeping the periodicity at the borders in mind, 4 different quadruple points initially exist in the simulation domain, one in the center, one at the edges and two at the horizontal and vertical boundaries.

The quadruple points are unstable versus splitting in two triple points. To induce this splitting a perturbation was necessary which was realized in two different

ways. First, a small amount of Gaussian distributed noise was added to the diffuse interface profile for each interface. The noise amplitude for this simulation and the following was chosen small enough not to increase the numerically determined surface energy significantly. Fig. 9 shows the temporal evolution for one simulation run, where a tiling of hexagons with 120° inner angle occurs (chart **c**). Due to the fixed square dimension of the domain, it is elongated vertically by a factor of $2/\sqrt{3}$ in comparison to the ideal hexagonal tiling.

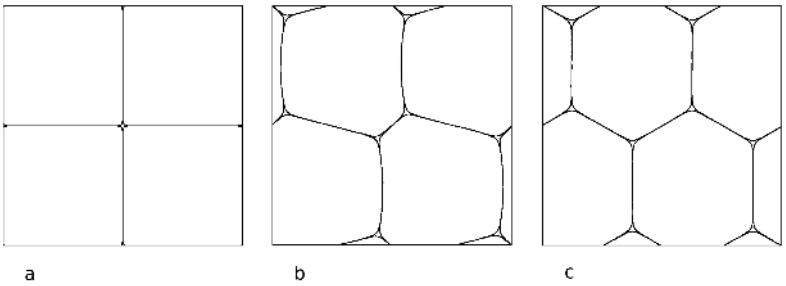

Fig. 9. 2D tiling of a square domain with 4 cells of equal area. The triple point separation is initiated by a small amount of noise on all diffuse interfaces. Contour line plots are given for simulation times 0.0, 0.0825, and 1.185 (**a** - **c**)

As a second method the perturbation of the quadruple points was realized by initially filling neighbored grid points in different quadrants with the same phase-field parameter. In this way the direction of the quadruple point splitting is fixed in advance. All combinations of directions in agreement with the periodicity were tested, leading to the four different tessellations depicted in Fig. 10. The left column indicates the enforced initial splitting directions. The temporal evolution of the surface energy for these four cases is given in Fig. 11. Scaling the energy of the hexagonal tiling in Fig. 10**a** to unity, the value for the surface energies of the configurations **b** - **d** were calculated to 1.028, 1.039, and 1.066.

The minimum energy configuration (chart **a**) is the same hexagonal structure as found after perturbing the interface with noise (see Fig. 9), and we conjecture that this is the solution to the above stated tessellation problem. The configuration with second lowest value is a combination of two regular pentagons with curved sides and two heptagons (adjoining in the center of chart **b**) with two sides only minor developed. This geometry resembles the Cairo pentagonal tiling consisting of 4 identical irregular pentagons. Giving to all quadruple points the identical splitting direction the distorted hexagonal structure in Fig. 10**c** establishes. The highest energy configuration is a combination of square-like objects in chart **d**, with convex and concave sides (the concave objects are in fact degenerated octagons). As in the case **b** the curved polygonal sides arise to establish the 120° angles according

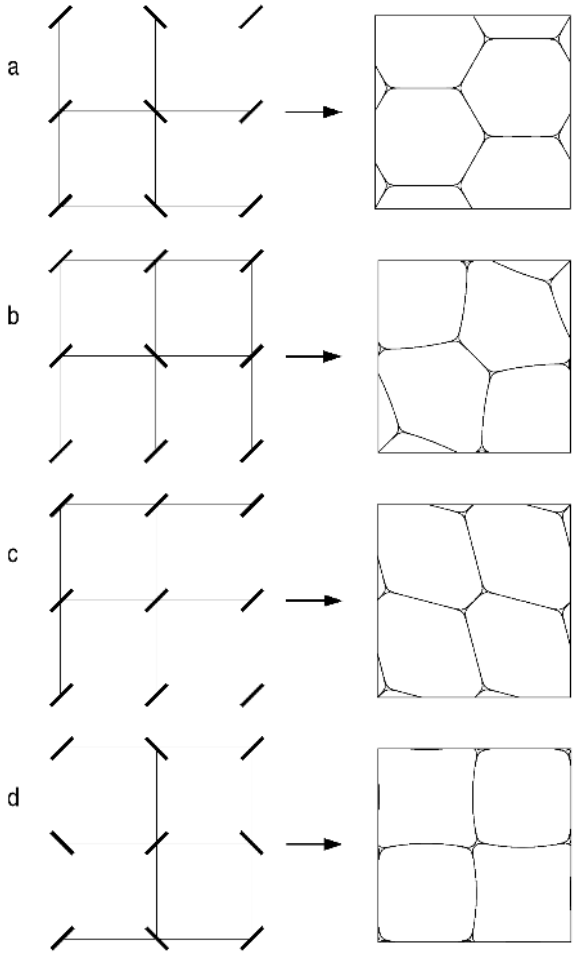

Fig. 10. The morphologies found in the 2D tessellation of a square domain with 4 cells, ordered with increasing surface energy from **a** - **d**: hexagon, pentagon/heptagon, distorted hexagon, and concave/convex squares. The quadruple points were perturbed on a grid cell scale with the initialized phase interface orientation marked as bold lines.

to the force balance condition (2.3). Due to the larger interface width used in the simulations, this configurations was only temporarily stable and switched after some time to the pentagon/heptagon configuration (cp. Fig. 11, dotted line).

4.4.2. *Tessellation in 3D*

For the simulations in 3D a computational domain of $100 \times 100 \times 100$ grid points was chosen. First, four squares in the form of tetragonal prisms were initiated with equal volumes. As expected an arrangement of hexagonal prisms establishes, with

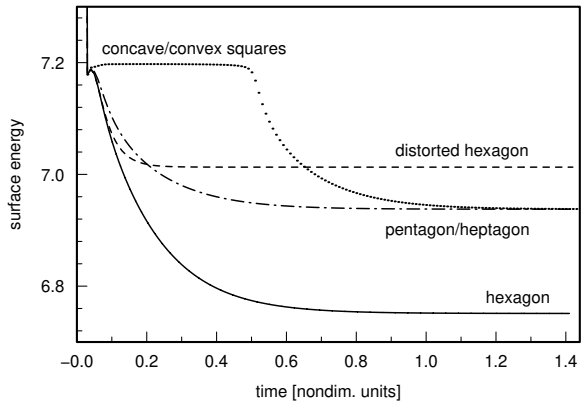

Fig. 11. Plot of the surface energy vs. time for the four tiling simulations from Fig. 10 **a** - **d**.

a cross sectional view as in the 2D case (Fig. 9**c**).

Second, the simulation domain was divided into 8 equal cubes and initiated with different phase-field parameters. The relaxation into the minimum energy configuration is shown in Fig. 12 at different time steps. Here, only the lower four grains are shown to allow for a better insight into the structure.

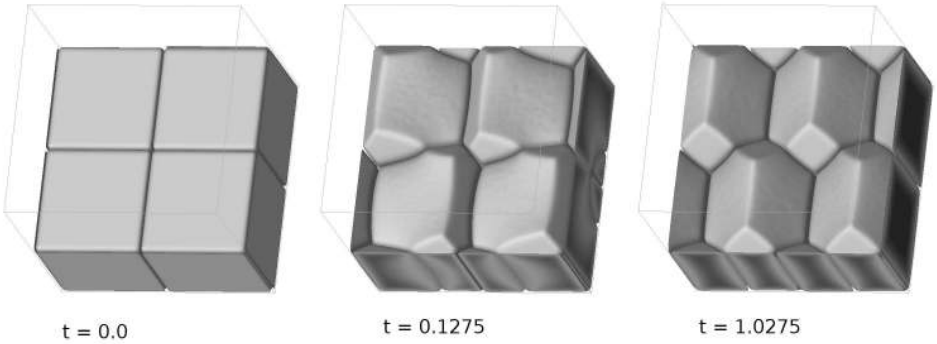

Fig. 12. Transformation of the initial checkerboard tiling into a pattern based on truncated octahedra as shown in Fig. 13. Only the lower 4 grains are shown.

A solution to the problem of partitioning the 3D space into equal volumes with minimum energy was proposed 1878 by Lord Kelvin[18] (we remark that a structure with less symmetry but with 0.3 % lower surface energy was found by D. Weaire and Phelon[20]). The building block is Kelvin's famous tetrakaidecahedron, a polyhedron with 14 sides. The tetrakaidecahedron results from a Voronoi partitioning

Fig. 13. Building block of the 3D cuboid tiling: A octahedron truncated at the edges in two different portions, revealing 2 small, 4 large square and 8 distorted hexagonal faces.

of the bcc crystal lattice and can be constructed by cutting the edges of an octahedron at a distance of $\frac{1}{6}\sqrt{2}\,l$, with l being the edge length of the octahedron. The hexagonal sides are not planar but slighly curved. In our simulation, a differently truncated octahedron emerges as a result (Fig. 13) with two larger square faces along one octahedral direction and four smaller faces in the perpendicular directions. The hexagonal faces are elongated but centrosymmetric. We conjecture that this form is the solution of the following problem. Partition the flat 3-torus into eight equal volumes with minimal interfacial area. The upper half of this cell (Fig. 13) strongly resembles the solution found for the minimum surface problem in a bee's honeycomb[19]: two arrays of ideal hexagonal faces on both sides of the honeycomb are opposed, and the problem consists in finding a minimal contact surface. In the bee's honeycomb the prisms are capped by three rhombi, whereas a better solution found by Fejes Tóth[19] is a combination of centrosymmetric hexagons and small rhombi, derived from a truncated octahedron.

To reproduce this problem, a 3D simulation domain of $100 \times 100 \times 116$ was chosen in order to make it possible that regular hexagons form on the faces. The periodic boundary conditions on two sides normal to the developing honeycomb were exchanged by Neumann boundary conditions. All other simulation parameters including the initial configuration were kept unchanged. In Fig. 14 (left) a top-view of the resulting interface structure is given, where again only the lower cells are shown. A single cell, depicted in Fig. 14 (right), clearly resembles the Tóth solution. Only a small rhombic distortion of the small squared faces is observed here. Some of the elongated hexagonal faces in the contact surface were examined geometrically and show a ratio of the long perimeter vs. the (perpendicular) height of 1.48 (Tóth solution: 1.5).

4.5. *Anisotropy in the surface energy: Platonic solids*

As a final application with a relation to grain growth the effect of an anisotropic surface energy was studied. Here, a faceted surface energy density was set as $a(\boldsymbol{\phi}, \nabla\boldsymbol{\phi}) = (\max_{1\le k\le n}\{(\phi_\alpha\nabla\phi_\beta - \phi_\beta\nabla\phi_\alpha)\cdot\vec{\eta_k}\})^2$ which results in crystalline

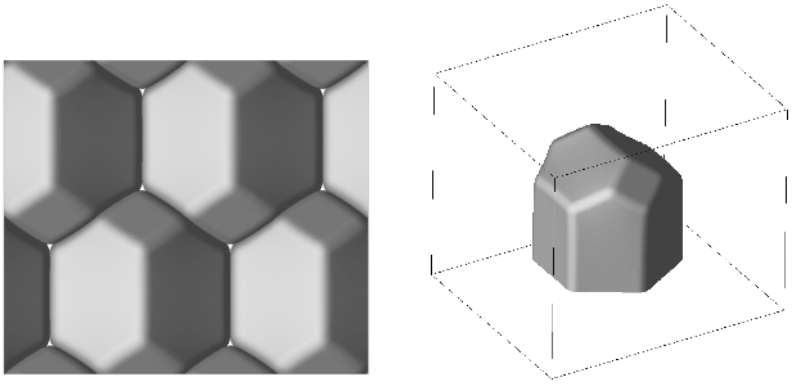

Fig. 14. Left: top view of the lower four cells of the 3D honeycomb structure using a numerical grid of laterally 116×100 points and vertically 100. Right: a single cell showing two elongated hexagonal and two small square faces.

shapes with flat faces and n edges in direction of the vectors η_k. As an example, we chose the edge vectors η_k to be the corners of the tetrahedron, the hexahedron, the octahedron, the dodecahedron, and the icosahedron, and studied the shape evolution of a spheroidal crystal into each that platonic bodies. In the simulation domain of $100 \times 100 \times 100$ grid cells an initially spherical grain was set with a radius of 30 cells. The volumes of both phases, the grain and the matrix phase, were preserved and the simulations carried out until no more change in the surface energy was recognizable.

In Fig. 16 the final shapes of all edge vector configurations are depicted after 12000 time steps. The transition time of the sphere into the final polygons decreases with increasing number of edges: for the solids **a** - **e** respectively 3000, 2750, 2000, 500, and 500 time steps were necessary to reach the final energy within 1 % of its final value. The edges along the regular polygons of their surface (triangles, squares, or pentagons) then exhibit a curvature whose radius scales with the diffuse interface width ε.

Appendix A. Derivation of the motion laws

In this appendix we briefly sketch how the motion laws (2.1) and the conditions (2.3) and (2.4) are obtained from an appropriate gradient flow of the energy (1.1) taking the constraints (1.2) into account.

An admissible configuration is a subdivision $S_\Omega := \{\Omega_1, \ldots, \Omega_M\}$ of Ω into subdomains with the properties as described at the beginning of Subsec. 2.1.1. The manifold of such admissible configurations is denoted by $\boldsymbol{N}$. Variations are based on deformations of the domain Ω. We define the tangential space on $\boldsymbol{N}$ in some element S_Ω to consist of objects $w = \{w_{\alpha\beta} : \Gamma_{\alpha\beta} \to \mathbb{R}\}_{\alpha<\beta}$ where $w_{\alpha\beta}$ is the deformation of $\Gamma_{\alpha\beta}$ in normal direction $\boldsymbol{\nu}_{\alpha\beta}$. We set $w_{\alpha\beta} := -w_{\beta\alpha}$ if $\alpha > \beta$ for

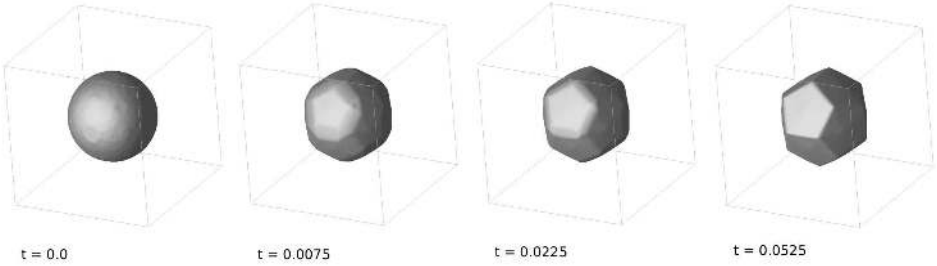

Fig. 15. Evolution of a sphere at specified simulation time into a dodecahedron. A faceted anisotropic surface energy density was used.

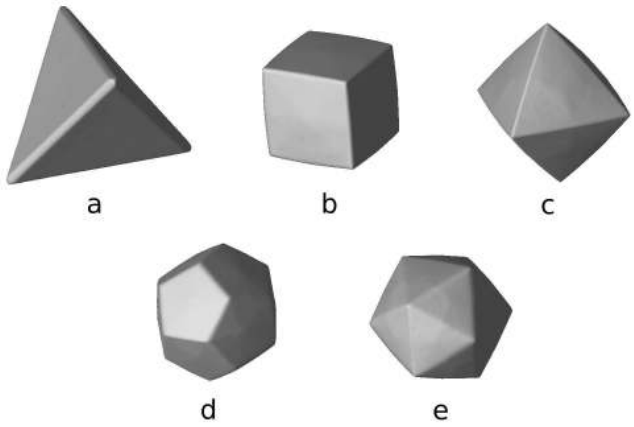

Fig. 16. Platonic solids as final configurations in the simulations with faceted anisotropic surface energy, **a** - **e**: tetrahedron, hexahedron, octahedron, icosahedron and dodecahedron.

simplifying the presentation. To avoid splitting of the sets $T_{\alpha\beta\delta}$ the $w_{\alpha\beta}$ have to fulfill the following conditions. If $\boldsymbol{w}_{\alpha\beta\delta}$ is the deformation of a point belonging to $T_{\alpha\beta\delta}$ then

$$\boldsymbol{w}_{\alpha\beta\delta} \cdot \boldsymbol{\nu}_{\alpha\beta} = w_{\alpha\beta}, \quad \boldsymbol{w}_{\alpha\beta\delta} \cdot \boldsymbol{\nu}_{\beta\delta} = w_{\beta\delta}, \quad \boldsymbol{w}_{\alpha\beta\delta} \cdot \boldsymbol{\nu}_{\delta\alpha} = w_{\delta\alpha}.$$

For two deformations $w = \{w_{\alpha\beta}\}_{\alpha<\beta}$ and $u = \{u_{\alpha\beta}\}_{\alpha<\beta}$ we define the product

$$(u, w) := \sum_{\alpha<\beta} \int_{\Gamma_{\alpha\beta}} m_{\alpha\beta} u_{\alpha\beta} w_{\alpha\beta} \, d\mathcal{H}^{d-1}$$

with positive weights $m_{\alpha\beta}$ which will become the kinetic coefficients in (2.1). Let us write the constraints (1.2) in the form

$$\mathcal{C}_\alpha(S_\Omega) := |\Omega_\alpha| - M_\alpha = 0, \quad \alpha = 1, \ldots, A,$$

and let $\mu_1, \dots, \mu_A$ be Lagrange multipliers for those conditions.

Given an admissible configuration S_Ω, its evolution $\partial_t S_\Omega$ is an element of the tangential space $T_{S_\Omega}\boldsymbol{N}$ on $\boldsymbol{N}$ in S_Ω, and it is defined by a gradient flow of the energy $\mathcal{F}_{SI}(S_\Omega)$ subject to the conditions $\mathcal{C}_\alpha(S_\Omega) = 0$, $\alpha = 1, \dots, A$:

$$(\partial_t S_\Omega, w) := -\Big\langle \frac{\delta \mathcal{F}_{SI}}{\delta S_\Omega}(S_\Omega), w \Big\rangle - \sum_{\alpha=1}^{A} \mu_\alpha \Big\langle \frac{\delta \mathcal{C}}{\delta S_\Omega}(S_\Omega), w \Big\rangle \tag{A.1}$$

has to hold for every $w \in T_{S_\Omega}\boldsymbol{N}$.

The computation of the variation of $\mathcal{F}_{SI}(S_\Omega)$ in direction w is analogous to the computation of its time derivative in the proof of Lemma 2.2. We obtain (compare with (2.7) and (2.8))

$$\begin{aligned}\Big\langle \frac{\delta \mathcal{F}_{SI}}{\delta S_\Omega}(S_\Omega), w \Big\rangle = &\sum_{\alpha<\beta} \int_{\Gamma_{\alpha\beta}} \big(\nabla_s \cdot D\gamma_{\alpha\beta}\big)\, w_{\alpha\beta} d\mathcal{H}^{d-1} \\ &+ \sum_{\alpha<\beta} \int_{\partial\Gamma_{\alpha\beta}} \Big(\gamma_{\alpha\beta}\boldsymbol{\tau}_{\alpha\beta} - \big(D\gamma_{\alpha\beta}\cdot\boldsymbol{\tau}_{\alpha\beta}\big)\boldsymbol{\nu}_{\alpha\beta}\Big)\cdot \boldsymbol{w}_{\partial\Gamma_{\alpha\beta}} d\mathcal{H}^{d-2}.\end{aligned}$$

The variation of $\mathcal{C}_\alpha$ in direction w is given by (compare with (2.5), this is the change in volume when deforming the interfaces $\Gamma_{\alpha\beta}$ of Ω_α by $w_{\alpha\beta}$ in direction $\boldsymbol{\nu}_{\alpha\beta}$)

$$\Big\langle \frac{\delta \mathcal{C}}{\delta S_\Omega}(S_\Omega), w \Big\rangle = \sum_{\beta=1}^{M} \int_{\Gamma_{\alpha\beta}} w_{\alpha\beta}.$$

Altogether, writing $\partial_t S_\Omega = \{v_{\alpha\beta}\}$ the definition (A.1) becomes

$$\begin{aligned}&\sum_{\alpha<\beta} \int_{\Gamma_{\alpha\beta}} m_{\alpha\beta} v_{\alpha\beta} w_{\alpha\beta} d\mathcal{H}^{d-1} \\ &= \sum_{\alpha<\beta} \int_{\Gamma_{\alpha\beta}} \big(\nabla_s \cdot D\gamma_{\alpha\beta}\big)\, w_{\alpha\beta} d\mathcal{H}^{d-1} - \sum_{\alpha=1}^{A}\sum_{\beta=1}^{M} \int_{\Gamma_{\alpha\beta}} \mu_\alpha w_{\alpha\beta} d\mathcal{H}^{d-1} \\ &+ \sum_{\alpha<\beta} \int_{\partial\Gamma_{\alpha\beta}} \Big(\gamma_{\alpha\beta}\boldsymbol{\tau}_{\alpha\beta} - \big(D\gamma_{\alpha\beta}\cdot\boldsymbol{\tau}_{\alpha\beta}\big)\boldsymbol{\nu}_{\alpha\beta}\Big)\cdot \boldsymbol{w}_{\partial\Gamma_{\alpha\beta}} d\mathcal{H}^{d-2}.\end{aligned} \tag{A.2}$$

Let us first look at the last line. In points belonging to a set $\Gamma_{\alpha\beta,ext}$ the deformation $\boldsymbol{w}_{\partial\Gamma_{\alpha\beta}}$ can be any vector tangential to $\partial\Omega$. After rotating the vector $\gamma_{\alpha\beta}\boldsymbol{\tau}_{\alpha\beta} - \big(D\gamma_{\alpha\beta}\cdot\boldsymbol{\tau}_{\alpha\beta}\big)\boldsymbol{\nu}_{\alpha\beta}$ by 90 degree in the plane spanned by $\boldsymbol{\tau}_{\alpha\beta}$ and $\boldsymbol{\nu}_{\alpha\beta}$ we obtain (2.4) as a necessary condition. Having this established the last line becomes

$$\sum_{\alpha<\beta<\delta} \int_{T_{\alpha\beta\delta}} \Big(\sum_{(i,k)\in\mathcal{A}_{\alpha\beta\delta}} -(D\gamma_{ik}(\boldsymbol{\nu}_{ik})\cdot\boldsymbol{\tau}_{ik})\boldsymbol{\nu}_{ik} + \gamma_{ik}(\boldsymbol{\nu}_{ik})\boldsymbol{\tau}_{ik}\Big)\cdot \boldsymbol{w}_{\alpha\beta\delta} d\mathcal{H}^{d-2}$$

which yields the force balance (2.3). With the convention (2.2) a short computation shows that

$$-\sum_{\alpha=1}^{A}\sum_{\beta=1}^{M} \int_{\Gamma_{\alpha\beta}} \mu_\alpha w_{\alpha\beta} = \sum_{\alpha<\beta} \int_{\Gamma_{\alpha\beta}} (\mu_\beta - \mu_\alpha) w_{\alpha\beta}.$$

Thus, (A.2) finally yields the motion law (2.1).

Acknowledgment

The financial support by the German Research Foundation, grant no. Ga 695/1-3, is gratefully acknowledged. We also thank the German Federal Ministery of Education and Research for funding our research work.

References

1. J.F. Blowey, C.M. Elliott, Curvature dependent phase boundary motion and parabolic double obstacle problems, Degenerate diffusions (Minneapolis, 1991), *IMA Vol. Math. Appl.* **47** (1993) 19–60.
2. K.A. Brakke, The surface evolver, *Experiment. Math.* **1** (1992) 141–165.
3. L. Bronsard, B. Stoth, Volume-preserving mean curvature flow as a limit of a nonlocal Ginzburg-Landau equation, SIAM J. Math. Anal. **28** (1997) 769–807.
4. C. Carter, A. Roosen, J. Cahn, J.E. Taylor, Shape evolution by diffusion and surface attachment limited kinetics on completely faceted surfaces, *Acta Metal. Mater.* **43** (1995) 4309–4323.
5. G. Dziuk, C.M. Elliott, Finite elements on evolving surfaces, *IMA J Numer Anal*, doi:10.1093/imanum/drl023.
6. J. Foisy, M. Alfaro, J. Brock, N. Hodges, J. Zimba, The standard double soap bubble in $\mathbb{R}^2$ uniquely minimizes perimeter, *Pacific J. Math.* **159** (1993) 47–59.
7. H. Garcke, R. Haas, B. Stinner, On Ginzburg-Landau type free energies for multiphase systems, in preparation.
8. H. Garcke, B. Nestler, B. Stoth, On anisotropic order parameter models for multiphase systems and their sharp interface limits, *Physica D* **115** (1998) 87–108.
9. H. Garcke, B. Nestler, B. Stoth, Anisotropy in multiphase systems: a phase-field approach, *Interfaces and Free Boundaries* **1** (1999) 175–198.
10. H. Garcke, B. Nestler, A mathematical model for grain growth in thin metallic films, *Math. Mod. Meth. Appl. Sc.* **10** (2000) 895–921.
11. H. Garcke, S. Wieland, Surfactant spreading on thin viscous films: nonnegative solutions of a coupled degenerate system, *SIAM J. Math. Anal.* **37** (2006) 2025–2048
12. M.E. Gurtin, Thermomechanics of Evolving Phase Boundaries in the Plane, *Oxford University Press* (1993).
13. M. Hutchings, F. Morgan, M. Ritoré, A. Ros, Proof of the double bubble conjecture, *Electronic Research Announcements of the Amer. Math. Soc.* **6** (2000) 45–49.
14. F. Morgan, M. Ritoré, Geometric measure theory and the proof of the double bubble conjecture, Global theory of minimal surfaces, *Clay Math. Proc.* **2**, Amer. Math. Soc., Providence, RI (2005) 1–18.
15. L. Qi, Jie Sun, A nonsmooth version of Newton's method, *Math. Programming* **58** (1993) 353–367.
16. J. Rubinstein, P. Sternberg, Nonlocal reaction-diffusion equations and nucleation, *IMA J. Appl. Math.* **48** (1992) 249–264.
17. J.E. Taylor, Mean curvature and weighted mean curvature, *Acta metall. mater.* **40** (1992) 1475–1485.
18. W. Thomson (Lord Kelvin), On the division of space with minimum partitional area, *Phil. Mag.* **24** (1887) 503.
19. L. Fejes Tóth, What the bees know and what they do not know. *Bull. Amer. Math. Soc.* **70** (1964) 468–481.
20. D. Weaire, R. Phelan, A counter-example to Kelvin's conjecture on minimal surfaces, *Forma* **11** (1996) 209–213, reprint of *Philos. Mag. Lett.* **69** (1994) 107-110.

21. M. J. Ward, Metastable bubble solutions for the Allen-Cahn equation with mass conservation, *SIAM J. Appl. Math.* **56** (1996) 1247–1279.